To:

Behnoush and Shervan

Abstract

The hydraulic headbox used in paper manufacturing machines has a two-dimensional contraction. It is believed that some of the mechanical properties of the produced paper depend on the flow inside this contraction. Problems as non-homogeneity and streaky structures of paper sheets are related to this flow. In order to determine the performance of different turbulence models in two-dimensional contractions, the turbulence characteristics along the contraction centreline were measured and compared to computational results using different turbulence models and to results from analytical methods in the literature. This study showed that the Reynolds stress model qualitatively predicts the flow well. However, the results were dependent on the upstream boundary condition for the rate of dissipation. Besides, it was observed that the performance of the $K-\epsilon$ model is very poor for this kind of flow.

In some applications of hydraulic headboxes turbulence producing vanes are mounted in the contraction zone. Also, in a special kind of paper manufacturing, by mounting separation vanes in the contraction zone, it is possible to put different components into separate layers of the paper sheet and thereby improve the sheet quality. However, the commercial introduction of forming of multi-layer printing and writing papers is held back due to large layer mixing in the jet of the headbox. This mixing is believed, to a large extent, to be the result of turbulent fluctuations in the wake behind the separation vanes.

The turbulence level and characteristics of these wakes depend, among other things, on the boundary layer that separates from the vanes. The development of this boundary layer was studied experimentally using the hot wire anemometer technique and it was found that because of the favourable pressure gradient the turbulent boundary layer relaminarises and becomes self-similar, before it reaches the end of the vane. Moreover, the turbulent wake behind the vane was investigated. It was observed that the wake can become self-similar although a universal velocity and length scale was not found. In addition, the mixing in the wake behind the vane was studied experimentally by heating the flow above the vane and measuring the temperature profiles downstream. It is a definite possibility that for any headbox configuration, there is an optimum vane length which leads to the lowest mixing.

The layer mixing in the stratified liquid jet of a headbox was modelled by a simple model using a commercial Navier-Stokes solver. A passive scalar was put in one of the fluid layers and its transport to the other layers was investigated. It was observed that the relative difference of the vane length and the contraction length was one of the most important factors. It was also shown that a vane shorter than the contraction gives unexpectedly low mixing. A quasi-one-dimensional model was developed to determine the shape of the separation vanes subjected to the fluid flow in a stratified headbox. It was observed that the results were dependent on vane bending stiffness, the relative velocity difference

at the contraction inlets, contraction geometry and the relative length difference of the vane and the contraction. This model was tested by comparing its results to the results of a Navier-Stokes solver using the commercial code CFX, and it was observed that they agree well.

Preface

This thesis studies the flow inside a two-dimensional contraction, in which the flow is contracted only in the vertical direction. This investigation consists of boundary layer, wake, and mixing inside the wake and is applicable to flow inside the hydrodynamic headbox of paper manufacturing machines.

- Paper I. Parsheh M. & Dahlkild A. A. 1997 Numerical modelling of mixing in stratified headbox jet. Presented at TAPPI engineering & Papermakers Conference Nashville, 1997 and a modified version to be submitted.
- Paper II. Parsheh M. & Dahlkild A. A. 1999 Modelling the flow around elastic guiding vanes in the converging zone of a headbox. Presented at TAPPI Engineering/Process and Product Quality Conference Trade Fair at Anaheim 1999, and a modified version is submitted to the Journal of Pulp and Paper Science.
- **Paper III**. Parsheh M., Dahlkild A. A. & Alfredsson P. H. 1999 Relaminarisation of a turbulent boundary layer in a two-dimensional contraction. To be submitted.
- **Paper IV**. Parsheh M., Talamelli A. & Dahlkild A. A. 2000 Turbulence characteristics of flow through two-dimensional contractions. To be submitted.
- **Paper V**. Parsheh M. 2000 Development and mixing of a flat plate wake in a two-dimensional contraction. To be submitted.

Contents

Chapter 1. Introduction	1
1. Paper manufacturing	1
2. The stratified headbox	1
3. The objectives of this thesis	2
Chapter 2. Basic equations	4
1. Equations governing the turbulent fluid flow	4
2. Aspects of boundary layer flow	5
2.1. The self-similar, laminar boundary layer	5
3. Aspects of wake flow	7
4. Aspects of passive scalar transport	9
Chapter 3. Computations	11
1. Mixing analysis	11
1.1. Effect of different turbulence models on mixing analysis	12
2. Flow around elastic guiding vanes	13
Chapter 4. Experiments	17
1. Experimental set-up	17
2. Flow at the centreline of contractions	18
2.1. Experimental study of flow through contractions	21
3. Relaminarisation of a turbulent boundary layer	25
3.1. The boundary layer measurement	27
4. Plane wakes subjected to favourable pressure gradient	30
4.1. Measurement of wakes in a two-dimensional contraction	30
4.2. Self-similarity of wakes subjected to pressure gradient	31
4.3. Wake characteristics	33
4.4. The analysis of mixing in the wake	35
Chapter 5. Concluding remarks	38
Division of work between authors	38
ACKNOWLEDGMENTS	40
Bibliography	41

CHAPTER 1

Introduction

1. Paper manufacturing

Paper is made by drainage of a fibre suspension to a wet web which is ultimately dried to a structure. To make paper was invented in China more than 2000 years ago. About 1000 years later, the method of producing paper manually was learned by Europeans. The method of producing paper by hand was not changed until the French revolution. At this time, the increase of paper demands together with the frequently strikes by paperworkers led to a shortage of paper products. Nicholas Louis Robert, a French engineer, invented the first paper machine which produced paper continuously. Since then, the paper machines have been successively developed and today modern paper machines can produce papers at a speed up to 2000 m/min. In a modern paper machine, fibre suspension flow out of a hydraulic headbox, in the form of a thin and wide liquid jet, is injected on one or between two permeable weaves, which are called wires (or 'fabrics'). It is believed that the flow conditions inside the headbox and liquid jet have a significant effect on the final paper quality, (see Aidun (1994) and Norman (1996)). A hydraulic headbox consists of a flow-spreader and a contraction of the flow in one direction and hereafter this contraction is called a 'two-dimensional' contraction. The main duty of a headbox is to distribute the fibre suspension uniformly across the wires. It means that, for instance, a flow from a pipe with diameter 800 mm will be changed to a 10 mm thick and 10,000 mm wide liquid jet with a very uniform velocity. The effect of the hydraulic headbox and liquid jet is not well understood. In final paper sheets, streamwise streaks can be found which could originate in the boundary layer of the two-dimensional contraction or in the liquid jet. The turbulence inside the headbox can effect the fibre orientation and fibre flocs and finally the quality of the produced sheet. The development of the turbulence characteristics inside two-dimensional contractions has not been studied in detail before. In some headboxes turbulence generating vanes are used to produce turbulence. The turbulence produced in the wake behind these vanes will help to break down the fibre flocs.

2. The stratified headbox

Using a special paper manufacturing technique, which is called 'stratified forming', the sheet quality can be improved by placing different components into different layers. To do this, one alternative is to form multi-layer papers from a

1

2 1. INTRODUCTION

single headbox, called 'stratified headbox'. In a stratified headbox, vanes inside a two-dimensional contraction separate different fluid layers. Figure 1.1 is the schematic of the stratified headbox used in EuroFEX pilot machine at STFI, Stockholm, Sweden. These elastic vanes are pinned at one end and are free to move at the other end. When the fluid flows into the converging part each vane is forced to a position which depends on its bending stiffness, and the distribution of surface forces from the fluid on both sides of the vane. The specific shape of the vanes is thus coupled to the flow field and headbox geometry. A stratified headbox forms a two-dimensional, free surface jet that consists of different layers which may have different velocities. The forming of multi-layer printing and writing papers from stratified headboxes, is held back due to the significant mixing of the different layers in the liquid jet.

In order to reduce mixing of fluid layers, Andersson (1982) used an air wedge downstream of the separation vane separating the fluid layers. Lloyd & Norman (1997) in an experimental study investigated the effect of vane length, vane trailing edge shape and the contraction opening shape on the mixing. They dyed the fibres in the centre layer blue. The "surface ply variation" was determined for various vane lengths, slice lips geometries and vane tip shapes by optically analysing the distribution of blue colour on the final paper surface. They found that longer vanes than the contraction produced small scale turbulence which caused mixing of the layers at fibre levels rather than at floc level. A sharp contraction immediately downstream of the vane tips reduced turbulent mixing, while parallel slice lips at the same position increased mixing. A narrower slice opening reduced layer mixing. Step expansions on both sides of the vanes a short distance upstream of the vane tips caused more layer mixing due to turbulence introduced by the steps.

The mixing of fluid layers in the liquid jet of a stratified headbox is believed to be, to a large extent, due to the turbulent fluctuations in the wake behind the vanes. However, the turbulence characteristics and level at these wakes depend, among other things, on the boundary layer development along the vanes. This boundary layer is subjected to a variable favourable pressure gradient and in some conditions can relaminarise.

3. The objectives of this thesis

The main aim of this thesis is to study the aspects of turbulent flow inside a two-dimensional contraction. The effect of this contraction on development of turbulent boundary layer, free stream turbulence, flat plate wake and mixing inside the wake is studied experimentally. Since the main goal is to determine the influence of the geometry, the experiments are carried out using air as the media. The experiments are performed in a small open wind tunnel and for the velocity field the hot wire anemometer technique is used. Comparisons have been done with previous experiments available in the literature and with well-known analytical theories and in some cases with performed numerical computations. Since

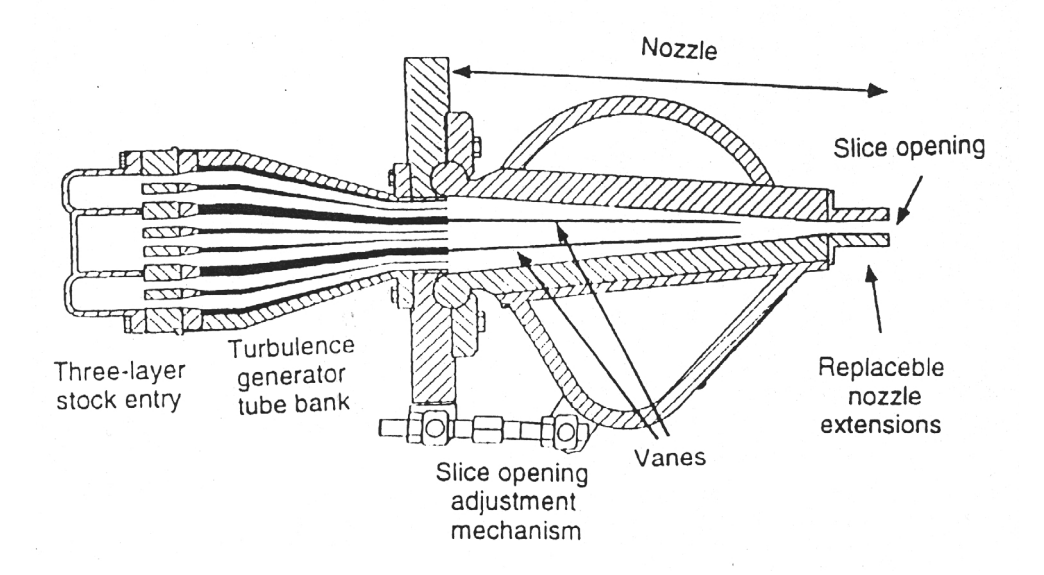


FIGURE 1.1. The schematic of the headbox used in EuroFEX pilot machine, STFI, Stockholm, Sweden.

the performance of turbulent models for this kind of flow has not been clarified earlier, the result of these turbulence models are compared to the measured data.

This thesis consists of five papers. Basic equations and short reviews of the theoretical background of the relaminarisation of a turbulent boundary layer, plane wakes subjected to a pressure gradient and the passive scalar transport are presented in chapter 2. Short summaries of the computational and the experimental results are presented in chapters 3 and 4, respectively. Despite the fact that the main body of this work has an experimental character, the experimental techniques are not discussed in this thesis.

CHAPTER 2

Basic equations

1. Equations governing the turbulent fluid flow

The governing equations for an incompressible turbulent flow of a viscous fluid are the Navier-Stokes equations and the continuity equation given by

$$\frac{\partial U_{i}^{'}}{\partial t} + U_{l}^{'} \frac{\partial U_{i}^{'}}{\partial x_{l}} = -\frac{1}{\rho} \frac{\partial P^{'}}{\partial x_{i}} + \nu \frac{\partial^{2} U_{i}^{'}}{\partial x_{l} \partial x_{l}}, \tag{2.1}$$

$$\frac{\partial U_i^{'}}{\partial x_i} = 0, \tag{2.2}$$

where $U_i^{'}$ an $P^{'}$ denote the instantaneous velocity and pressure and ρ and ν are the fluid density and kinematic viscosity, respectively. Reynolds decomposed the velocity and pressure into mean and fluctuating parts, i.e. $U_i^{'} = U_i + u_i$ and $P^{'} = P + p$ and inserted them into the Navier-Stokes equations and took the ensemble average. He obtained:

$$\frac{\partial U_i}{\partial t} + U_l \frac{\partial U_i}{\partial x_l} = -\frac{1}{\rho} \frac{\partial P}{\partial x_i} + \frac{\partial}{\partial x_l} \left(\nu \frac{\partial U_i}{\partial x_l} - \overline{u_i u_l} \right), \tag{2.3}$$

$$\frac{\partial U_i}{\partial x_i} = 0. {(2.4)}$$

The correlation $-\rho \overline{u_i u_l}$ is called the Reynolds stress tensor and is the result of the non-linear advective term in equation 2.1. Through this term the details of the turbulence make their imprint upon the mean velocity profile U_i . Due to the averaging of the Navier-Stokes equations we have lost information about the flow details and effect of the turbulent structure is distilled into the Reynolds stresses. Since the Reynolds stresses are unknown, the number of equations are insufficient to solve the problem. This is called the closure problem and implies that we need transport equations for Reynolds stresses which are presented by:

$$\frac{\partial \overline{u_{i}u_{j}}}{\partial t} + U_{l} \frac{\partial \overline{u_{i}u_{j}}}{\partial x_{l}} = -\overline{u_{i}u_{l}} \frac{\partial U_{j}}{\partial x_{l}} - \overline{u_{j}u_{l}} \frac{\partial U_{i}}{\partial x_{l}} + \frac{\overline{p}}{\rho} \left(\frac{\partial u_{i}}{\partial x_{j}} + \frac{\partial u_{j}}{\partial x_{i}} \right) - 2\nu \frac{\overline{\partial u_{i}}}{\partial x_{l}} \frac{\partial u_{j}}{\partial x_{l}} - \frac{\partial}{\partial x_{l}} \left(\overline{u_{i}u_{j}u_{l}} + \frac{\overline{p}}{\rho} (u_{i}\delta_{jl} + u_{j}\delta_{il}) - \nu \frac{\partial}{\partial x_{l}} \overline{u_{i}u_{j}} \right), \quad (2.5)$$

where the left-hand-side of equation 2.5 denotes the rate of change in a position which follows the mean velocity field. The first two terms in the right-hand-side of equation 2.5 show the production of Reynolds stresses. The third and fourth terms in the right-hand-side of this equation are the pressure-strain and viscous dissipation rate, respectively. The last term is a diffusion term and contains both turbulent and molecular terms. By this equation the closure problem is transferred to other moments of the fluctuating quantities.

2. Aspects of boundary layer flow

If U and V denote the streamwise and cross-streamwise mean velocity components, respectively, a simplified form of continuity and Navier-Stokes equations which represent the two-dimensional laminar boundary layer become

$$\frac{\partial U}{\partial x} + \frac{\partial V}{\partial y} = 0, \tag{2.6}$$

$$U\frac{\partial U}{\partial x} + V\frac{\partial U}{\partial y} = U_e \frac{dU_e}{dx} + \nu \frac{\partial^2 U}{\partial y^2}, \qquad (2.7)$$

where U_e denotes the local streamwise mean velocity of the external flow which is assumed to be constant at any streamwise position. The boundary conditions are U=V=0 for y=0, and $U=U_e$ for $y\longrightarrow\infty$. The displacement and the momentum loss thickness are defined as,

$$\delta^* = \int_0^\infty \left(1 - \frac{U}{U_e} \right) dy \; ;$$

$$\theta = \int_0^\infty \frac{U}{U_e} \left(1 - \frac{U}{U_e} \right) dy,$$

respectively. The boundary layer shape factor is defined as

$$H = \frac{\delta^*}{\theta}$$
.

The local skin friction coefficient is given by:

$$\frac{1}{2}c_f = \frac{d\theta}{dx} + \frac{dU_e}{dx}\frac{1}{U_e}(\delta^* + 2\theta). \tag{2.8}$$

2.1. The self-similar, laminar boundary layer. For the flow through a two-dimensional contraction with the primed coordinate shown in figure 2.1, U_e is given by

$$U_e(x') = -\frac{q}{r'\alpha},\tag{2.9}$$

2. BASIC EQUATIONS

6

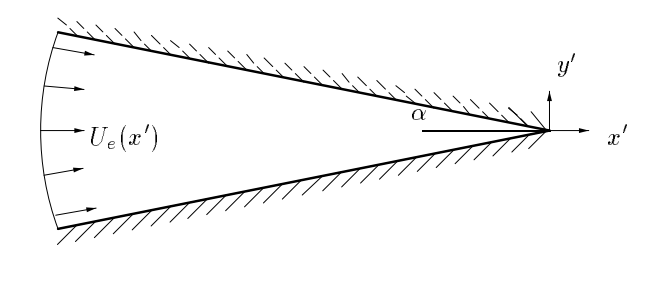


FIGURE 2.1. Flow in a converging channel.

where q is half the flow rate per unit width in the channel and α is the half angle of the contraction. The coordinate system origin is according to Fig. 2.1 at the apex of the continuation of the contraction.

In the self-similar solution presented next, no additional boundary condition may be specified. For the external flow velocity in (2.9), a self-similar boundary layer solution of (2.6), (2.7) is available from the Falkner-Skan family of equations for which the streamfunction is of the form

$$\psi(x', y') = \sqrt{-\nu x' U_e} f(\eta), \qquad (2.10)$$

and in our case

$$\eta = \frac{y'}{\sqrt{Kx'^2}},\tag{2.11}$$

where K is the acceleration parameter defined above and in our case is constant equal to $\frac{\nu \tan \alpha}{U_e h} = \frac{\nu \alpha}{q}$. The velocity components are thus given by

$$u = U_e f' \; ; \qquad v = -\sqrt{K} U_e \eta f', \tag{2.12}$$

and an equation for f is obtained by inserting (2.12) into (2.7) which yields

$$f''' - f'^2 + 1 = 0, (2.13)$$

the boundary conditions are f'=0 at $\eta=0$, and f'=1 and f''=0 at $\eta\longrightarrow\infty$.

$$f' = \frac{u}{U_e} = 3 \tanh^2 \left(\frac{\eta}{\sqrt{2}} + c\right) - 2.0,$$
 (2.14)

where $c = \tanh^{-1} \sqrt{\frac{2}{3}} = 1.146$. This is one of the few cases where the boundary layer can be solved analytically.

Non-dimensional properties such as shape factor, H, and local skin friction, c_f , for a self-similar boundary layer are constant. The Reynolds number is defined as $Re = U_e h/\nu$, where h is half the channel height. The acceleration parameter defined as $K = \frac{\nu}{U_e^2} \frac{dU_e}{dx}$ for the two-dimensional contraction depends on the contraction half angle, α , and the flow Reynolds number R_e as:

$$K = \frac{\tan \alpha}{Re}.\tag{2.15}$$

3. Aspects of wake flow

Considering the wake and the coordinate system shown in Fig. 2.2, if all viscous and normal turbulent stresses in the averaged Navier-Stokes equations are neglected, the two-dimensional turbulent wake equations read

$$\frac{\partial U}{\partial x} + \frac{\partial V}{\partial y} = 0, \tag{2.16}$$

$$U\frac{\partial U}{\partial x} + V\frac{\partial U}{\partial y} = U_e \frac{dU_e}{dx} + \frac{\partial (-\overline{u}\overline{v})}{\partial y}, \qquad (2.17)$$

where in equation 2.17, it is assumed that the changes of the static pressure inside the wake is equal to that of the external flow which is valid for shallow wakes. Assuming a shallow wake, of which the maximum value of the velocity defect is much smaller than the local external velocity $U_e - U \ll U_e$, and inserting equation 2.16 into equation 2.17 one obtains

$$U_e \frac{\partial (U_e - U)}{\partial x} - U'_e y \frac{\partial (U_e - U)}{\partial y} + U'_e (U_e - U) = \frac{\partial \overline{u}\overline{v}}{\partial y}.$$
 (2.18)

Townsend (1956) introduced the following self-similar coordinates

$$U_e(x) - U(x, y) = U_s(x)f(\eta),$$
 (2.19)

$$\overline{uv}(x,y) = -U_s^2 g(\eta), \qquad (2.20)$$

$$\eta = \frac{y}{l(x)},\tag{2.21}$$

where U_s is the maximum value of the velocity defect and l is the cross-stream scale which is defined as the distance between the centreline and the position at which $U_e - U$ is $\frac{1}{2}U_s$, shown in Fig. 2.2. Inserting equations 2.19 and 2.20 in equation 2.18 gives

$$\left\{\frac{1}{U_s}\frac{d(U_e l)}{dx}\right\}\eta f' - \left\{\frac{l}{U_s^2}\frac{d(U_e U_s)}{dx}\right\}f = g',\tag{2.22}$$

2. BASIC EQUATIONS 8

where primes on f and g denote differentiation with respect to η . The selfsimilarity requires that the coefficients of $\eta f'$ and f to be independent of x. This leads to the fact that the following quantity for the velocity profiles of a selfsimilar shallow wake should be independent of x (Narasimha & Prabhu (1971))

$$M = U_e^2(x)U_s(x)l(x). (2.23)$$

The constancy of M implies that the coefficients of (2.22) become equal. Narasimha & Prabhu (1971) used the following expressions

$$\overline{uv} = \nu_T \frac{\partial (U_e - U)}{\partial y},\tag{2.24}$$

$$\nu_T = k_0 U_s l, \tag{2.25}$$

in which k_0 is a universal constant and equal to

$$k_0 = \frac{\left\{\frac{1}{U_s} \frac{d(U_e l)}{dx}\right\}}{2 \ln 2} = \frac{\left\{-\frac{l}{U_s^2} \frac{d(U_e U_s)}{dx}\right\}}{2 \ln 2}$$
(2.26)

After solving equation 2.22 one can obtain

$$f(\eta) = \exp(-\eta^2 \ln 2). \tag{2.27}$$

For two-dimensional wakes the production of Reynolds stress components in (2.5) are simplified to:

$$P_{11} = -2\overline{u^2}\frac{\partial U}{\partial x} - 2\overline{u}\overline{v}\frac{\partial U}{\partial y},\tag{2.28}$$

$$P_{22} = 2\overline{v^2}\frac{\partial U}{\partial x} - 2\overline{u}\overline{v}\frac{\partial V}{\partial x},\tag{2.29}$$

$$P_{12} = -\overline{v^2} \frac{\partial U}{\partial y} - \overline{u^2} \frac{\partial V}{\partial x}.$$
 (2.30)

For the case of two-dimensional contractions the energy production terms of different components become:

$$P_{11} = -2\overline{u^2}\frac{\partial U}{\partial x},\tag{2.31}$$

$$P_{22} = 2\overline{v^2} \frac{\partial U}{\partial x},$$
 (2.32)
 $P_{33} = 0,$ (2.33)

$$P_{33} = 0, (2.33)$$

and the production term for the turbulent kinetic energy reads

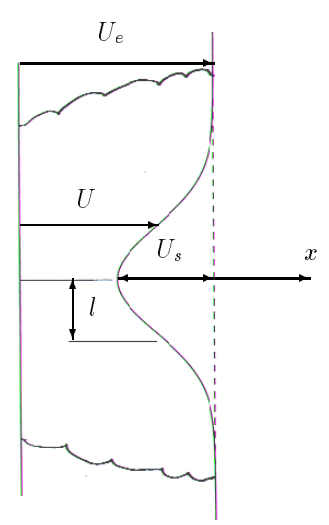


FIGURE 2.2. Plane wake inside a contraction.

$$P_k = (\overline{v^2} - \overline{u^2}) \frac{\partial U}{\partial x}.$$
 (2.34)

4. Aspects of passive scalar transport

The governing equations for a passive scalar are similar to those of the velocity field of incompressible flow. If Θ' is the instantaneous passive scalar the conservation equation of a passive scalar reads

$$\frac{\partial \Theta'}{\partial t} + U_l' \frac{\partial \Theta'}{\partial x_l} = \alpha \frac{\partial^2 \Theta'}{\partial x_l \partial x_l}, \tag{2.35}$$

where α is the molecular diffusivity. As is obvious this equation has no pressure term and thus, the pressure field and the scalar field are not directly related. In analogy with the Reynolds decomposition of the velocity field the instantaneous scalar field may be divided into a mean part and a fluctuating part, $\Theta' = \Theta + \theta$. The transport equation of the mean scalar is obtained by inserting this decomposition into equation 2.35 and taking the ensemble average, which gives

$$\frac{\partial \Theta}{\partial t} + U_l \frac{\partial \Theta}{\partial x_l} = \frac{\partial \left(\alpha \frac{\partial \Theta}{\partial x_l} - \overline{u_l \theta} \right)}{\partial x_l}.$$
 (2.36)

10 2. BASIC EQUATIONS

The scalar flux term, $\overline{u_l\theta}$, or Reynolds-flux term in analogy with the Reynolds stress, is due to the non-linear advection term in equation 2.35 and leaves equation 2.36 unclosed. The transport equation for the scalar flux is given by

$$\frac{\partial \overline{u_i \theta}}{\partial t} + U_l \frac{\partial \overline{u_i \theta}}{\partial x_l} = -\overline{u_i u_l} \frac{\partial \Theta}{\partial x_l} - \overline{u_l \theta} \frac{\partial U_i}{\partial x_l} + \overline{\frac{p}{\rho} \frac{\partial \theta}{\partial x_i}} - (\alpha + \nu) \overline{\frac{\partial \theta}{\partial x_l} \frac{\partial u_i}{\partial x_l}} \\
- \frac{\partial}{\partial x_l} \left(\overline{u_i u_j \theta} + \overline{\frac{p}{\rho} \theta \delta_{il}} - \alpha \overline{\frac{\partial \theta}{\partial x_l} u_i} - \nu \overline{\theta} \overline{\frac{\partial u_i}{\partial x_l}} \right), \quad (2.37)$$

which is in analogy to the transport equations for Reynolds stresses. The first two terms on the right hand side of these equations are production terms and the third term denotes a pressure scalar-gradient correlation term. The fourth and fifth terms denote the viscous and diffusive dissipation and turbulent and molecular diffusion, respectively.

In a turbulent plane wake when the Reynolds number is sufficiently large, the diffusive transport of a passive scalar is negligible and the stationary transport equation becomes

$$U\frac{\partial\Theta}{\partial x} + V\frac{\partial\Theta}{\partial y} = -\frac{\partial\overline{v\theta}}{\partial y} - \frac{\partial\overline{u\theta}}{\partial x}.$$
 (2.38)

In analogy with the production terms of turbulent components the production term of the transport of the scalar flux is defined as

$$P_{u_i\theta} = -\overline{u_i u_l} \frac{\partial \Theta}{\partial x_l} - \overline{u_l \theta} \frac{\partial U_i}{\partial x_l}, \qquad (2.39)$$

and the production term of half the scalar variance, a quantity corresponding to the turbulent kinetic energy reads

$$P_{\theta} = -\overline{u_i \theta} \frac{\partial \Theta}{\partial x_i},\tag{2.40}$$

which is proportional to the mean scalar gradient.

CHAPTER 3

Computations

1. Mixing analysis

The mixing in the liquid jet of a stratified headbox was studied numerically. In this study the flow a few centimeters upstream of the contraction outlet and the liquid jet were modelled and the vanes were assumed to be fixed. The contraction angle and the vane geometry as well as the flow specifications were varied and the mixing process for different cases were compared. In order to study the mixing process, a passive scalar component was 'dyed' into the middle fluid layer and its transport was studied. Here, the mean passive scalar mass fraction is denoted by ϕ . Although fibre suspension flow shows highly non-Newtonian properties, the fluids properties were, for simplicity, chosen as water at room conditions. In order to quantify the mixed region, the defect passive scalar flux density in the dyed fluid layer, $(1 - \phi(x, y))u(x, y)$, is integrated across the middle layer and distributed over a rectangle with the area $1 \times \delta(x)\bar{u}(x)$. The quantity $\delta(x)$ is a measure of the mixed region at any x-position and shows the development of the mixed region along the jet. It is thus defined as

$$\delta(x) = \frac{1}{\bar{u}(x)} \int_0^{h(x)} (1 - \phi(x, y)) u(x, y) dy$$
 (3.1)

where h(x) is half the middle fluid layer thickness defined as

$$Q_m = \int_0^{h(x)} u(x, y) dy. {(3.2)}$$

Here Q_m is half the volume flow per unit width of the jet in the middle layer. Further, a dimensionless $\delta(x)$ is defined as

$$\bar{\delta}(x) = \frac{\delta(x)}{h(x)} \tag{3.3}$$

which measures the mixed region of the middle layer to its thickness. The $K-\varepsilon$ model was used and since this model has poor performance in computing largely contracted flows (Parsheh *et al.* (2000)), a minor part of the contraction with a maximum contraction ratio of 3 was modelled.

One of the main issues studied in this work was the effect of vane length, and thus different pressure gradient variations, on the mixing. It was shown that

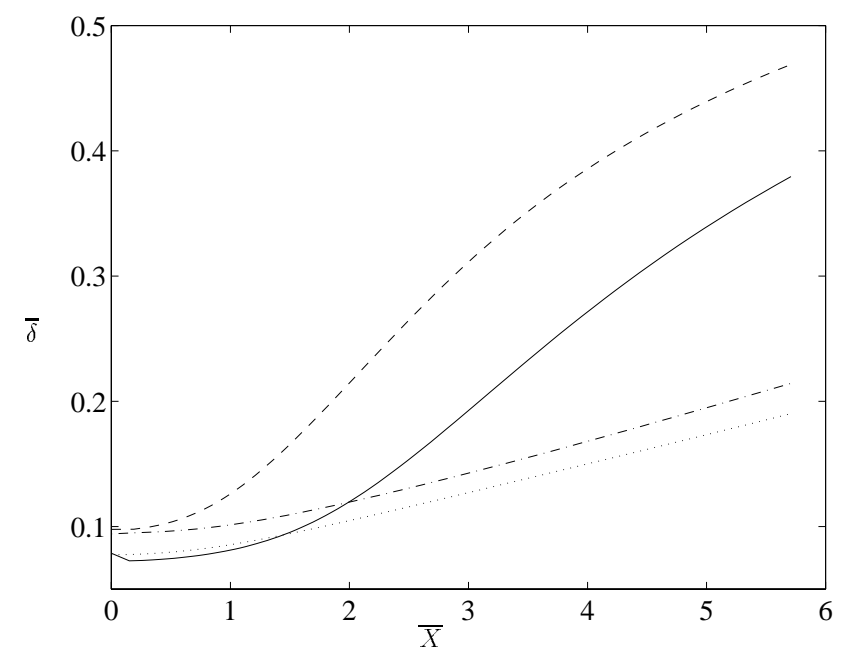


FIGURE 3.1. The development of $\overline{\delta}$ vs. dimensionless position in the liquid jet. (- - -) RVL = -100 mm $K - \epsilon$ model, (—) RVL = -50 mm $K - \epsilon$ model, (- · -) RVL = -100 mm DRST model and (· · ·) RVL = -50 mm DRST model.

when the vane length is shorter than the contraction length it can lead to a less mixed state of the efflux from the free jet than that obtained with a vane of equal or greater length than the contraction. However, with a too short vane the longer time that different layers were in contact resulted in higher mixing. Thus, there is a possibility to find an optimum vane length for which the purity of the layers in the efflux of the jet are highest at some desired point downstream of the contraction. Since a model of a shorter vane than those reported in this work needs modelling of a longer part of the contraction, the potentially poor performance of the turbulence models for large contraction ratios can give results that are misleading. Therefore, in the following part results from two different turbulence models are studied and their effects on mixing compared.

1.1. Effect of different turbulence models on mixing analysis. The typical result of this study is shown in Fig. 3.1. In this analysis a complete contraction, with contraction ratio 13.8, was modelled and two different vane lengths were studied. The quantity RVL denotes the distance between the plate trailing edge and the contraction outlet. As this figure shows the mixing of the cases in which the $K - \epsilon$ model were used are much larger than that of the Differential

Reynolds stress cases. However, when a comparison between different geometries is considered both turbulence models predict the same tendency that the configuration with the shorter vane gives higher mixing in this case. One should note that unlike these computations, the cases presented in paper I covered only a minor part at the end of the contraction and, thus, the effect of exaggeration of the kinetic energy by the $K-\epsilon$ model was limited. It is interesting to note that in both configurations the mixing due to both turbulence models at contraction outlet are almost equal and the layer mixing becomes significant in the jet where the pressure gradient is zero.

This simple study shows that, when a comparison between different configurations is considered, the choice of turbulence model may have no major effect on the mixing analysis. In order to be precise and avoid any uncertainty, the turbulent flow along the contraction centreline was measured and the performance of different turbulence models were studied. This study seemed to be inevitable since flow through the contracting zone of headboxes had been modelled widely but no investigation on the performance of different turbulence models for this flow was performed. Since the lowest mixing was obtained for vanes shorter than the contraction length, some parts of this thesis are focused on wakes developing in contractions and the mixing processes in these wakes. Since the flow condition in the boundary layer at vane trailing edge has a significant effect on the wake characteristics, this boundary layer is studied experimentally.

From computations in this study it was also observed that due to the contraction of the free jet, the mean velocities of the outer jet layers differed from the middle layer. In order to obtain equal velocities in the jet layers, the middle layer should have slightly higher inlet velocity than the outer layers. This was named as the 'concept of modified flow rates'. The vanes shape and position along the contraction as well as the layers outlet velocities from the contraction depend on the inlet flow rates and the vane bending stiffness. Thus, a complete study of the mixing in the liquid jet, for a specific contraction, would include finding the vane bending stiffness and inlet flow rates which force the elastic vane to a position which lead to lowest mixing. Because of the nature of this task, which requires a 'trial and error' procedure, and therefore needs plenty of attempts, we need a program which can determine the vane position along the contraction at shortest possible time. Therefore, a quasi-one-dimensional model was developed and some important cases studied. The next section is assigned to review this study.

2. Flow around elastic guiding vanes

The position and form of the elastic vanes inside the converging zone of headboxes are a priori unknown. A quasi-one-dimensional method was implemented to determine them as functions of geometry and flow parameters. The vanes are pinned at one end and free to move at the other end. Thus, if there is no flow in the headbox they lie on the bottom of the contraction and when there is flow

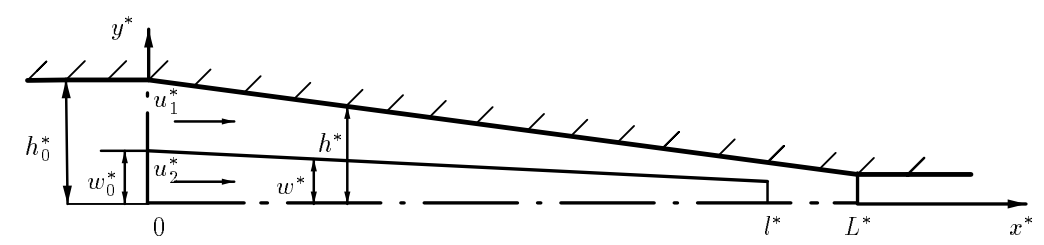


FIGURE 3.2. Sketch of headbox geometry with elastic vane. Due to symmetry only the upper half part of the headbox is shown; Plane of symmetry (- · -).

they will be forced into specific shapes along the headbox. The vane length can be equal to the contraction length or it can be arbitrarily longer or shorter. A headbox may have several vanes. A simple sketch of an elastic vane inside a contraction is shown in Fig. 3.2. In this figure it is assumed that the headbox has two vanes whose fixed points are symmetrical with respect to the contraction centreline. The vane weight has been ignored in this study due to the negligible effect compared to the hydrodynamic forces. Because of the two-dimensional geometry and flow, we ignore the effect of the side walls and the vane can be considered as a narrow 'beam'. Let $y^* = h^*(x^*)$ be the equation of the contraction where $h^*(x^*)$ can be an arbitrary function. We introduce $y^* = w^*(x^*)$ as the equation of the vane position in the contraction. The quantity w_0^* denotes the fixed position of the vane at $x^* = 0$. Now, the equation of the vane position reads

$$E^*I^*\frac{d^4w^*}{dx^{*4}} = \Delta p^*(x^*; w^*(x^*)), \tag{3.4}$$

where Δp^* denotes the difference of the static pressure on the upper and lower side of the vane. The product E^*I^* is the bending stiffness of the vane where E^* is the vane's module of elasticity and I^* the principle moment of inertia of the cross-sectioned area of the vane with respect to an axis perpendicular to the xy-plane. The boundary conditions for equation 3.4 become

$$x^* = 0 : w^* = w_0^* , E^* I^* \frac{d^2 w^*}{dx^{*2}} = 0,$$
 (3.5)

$$x^* = l^* : E^* I^* \frac{d^2 w^*}{dx^{*2}} = 0 , E^* I^* \frac{d^3 w^*}{dx^{*3}} = 0.$$
 (3.6)

Using the finite difference method this equation was solved and different flow cases and vane characteristics were studied. Figure 3.3 shows one sample of the results. This simple quasi-one-dimensional model showed that when the contraction body was linear at equal inlet velocities to different layers, the shape and position of the elastic vane do not depend on the vane bending stiffness. The vane remains straight and outlet velocities become equal. In the case of unequal

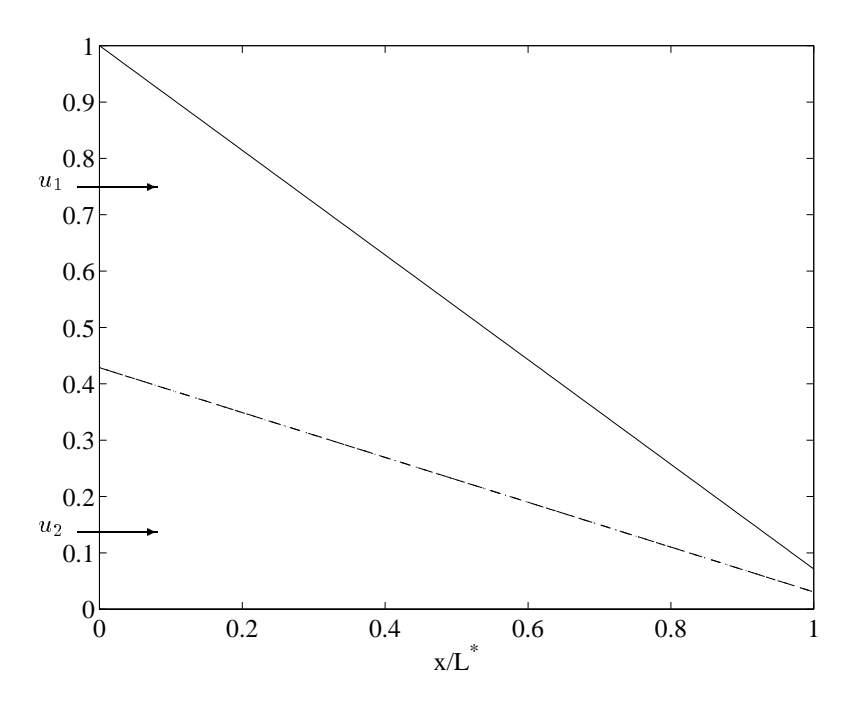


FIGURE 3.3. The vane position along the contraction $u_1^* = u_2^* = 1.3$ m/s for vanes: $E^*I^* = 0$ Nm^2 (- · -); $E^*I^* = 3600$ Nm^2 (- - -); $E^*I^* = 4.86 \times 10^4$ Nm^2 (· · ·); headbox body (—). The outlet velocities for vanes become $u_{e1}^* = u_{e2}^* = 18.2$ m/s.

inlet velocities the vane shape, position and outlet velocities depend on the vane bending stiffness.

In the case of non-linear contraction body it was observed that even at equal inlet velocities, unlike the case of a linear body, the shape of the vane becomes curved. The outlet flow velocities become unequal unless the vane stiffness is negligible. Figure 3.4 shows an example of computations when the contraction body is a second degree polynomial function.

The results of this model were compared to the results of a commercial Navier-Stokes solver and it was observed that they agree well.

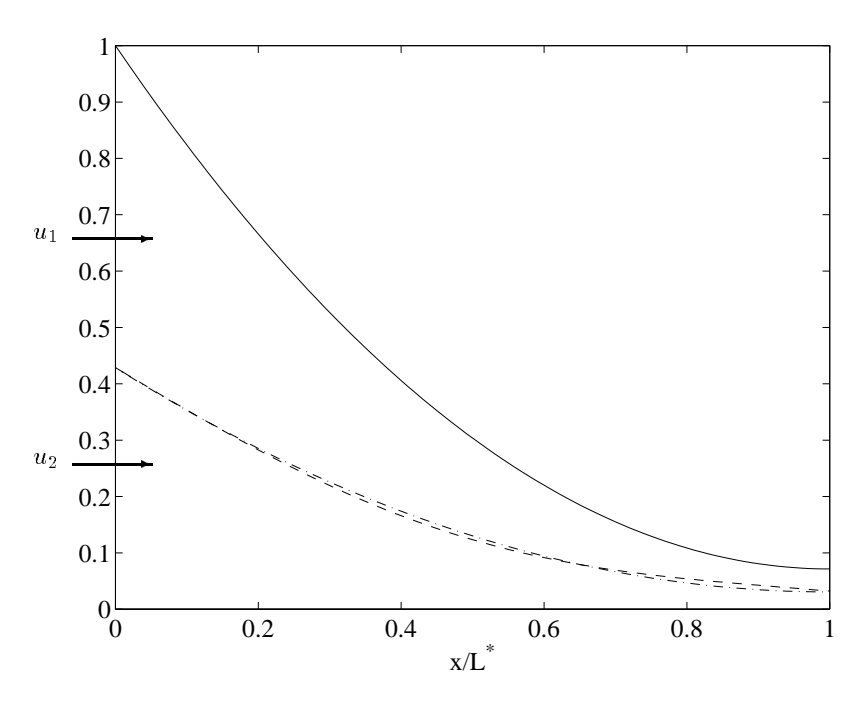


Figure 3.4. The vane position along the contraction when the contraction body, h^* (—), is a non-linear function.

CHAPTER 4

Experiments

In this thesis three different series of experiments are reported which were performed in order to study the flow inside a two-dimensional contraction, in which the flow is only contracted in one direction. In the first experiment series the turbulent flow along the centreline of a two dimensional contraction was measured and the effect of the inlet turbulent scale and contraction ratio were investigated. In the second experiment, the development of a boundary layer on a plate mounted along the centreline of the same contraction was measured while the wake behind the plate was studied in the third experiment.

1. Experimental set-up

The experiments were performed in a small open wind tunnel at KTH, in Stockholm. The test section presented in Fig. 4.1 was a two-dimensional contraction with adjustable half angle. The typical variation of mean streamwise rate of strain is presented in Fig. 4.2. In the boundary layer and wake measurements a plate as shown in Fig. 4.3 was mounted at the centreline of the test section. The free-stream turbulence was generated by means of grids installed upstream of the converging channel. The grids were of the form of bi-plane square-mesh

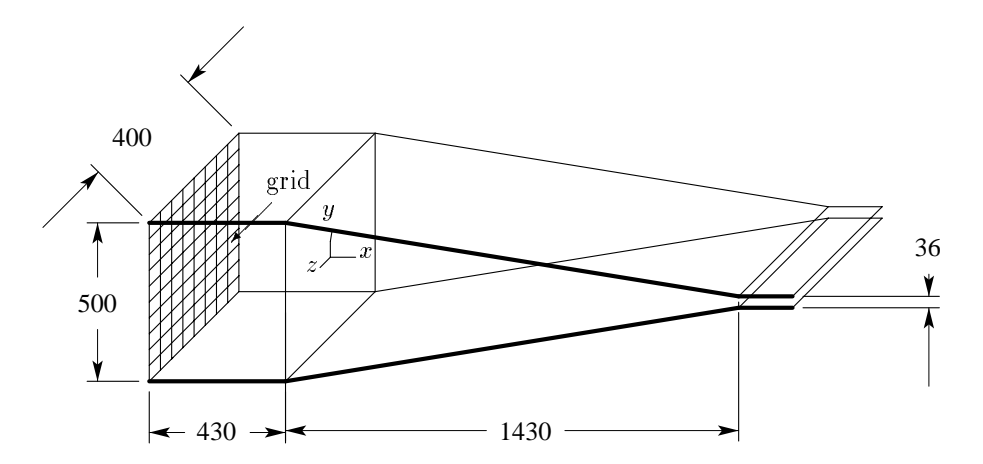


FIGURE 4.1. Outline of the test section used in different experiment series, dimensions in mm.

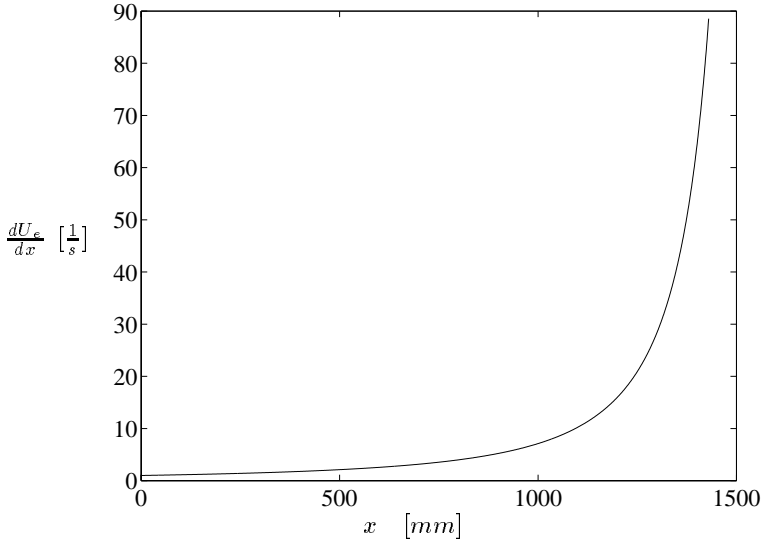


FIGURE 4.2. The typical downstream variation of mean streamwise rate of strain along the contraction.

arrays of square bars. The mesh size and bar diameter of the first (smaller) grid, which hereafter is called grid gs, were 23 and 4 mm respectively, giving a solidity of 0.32 (the solidity is defined as the grid geometric blockage area over the total area). The dimensions of the second (larger) grid, which is called grid gl, were 34 mm and 6 mm respectively which gave the same solidity as grid gs. The flow velocity was measured with a constant-temperature hot-wire anemometer (CTA). The wires were calibrated with a Prandtl tube in the constant height channel downstream of the contraction. For each wire a calibration function of the form

$$U = k_1 (E^2 - E_0^2)^{1/n} + k_2 (E - E_0)^{1/2}, (4.1)$$

was used, where E and E_0 are the anemometer output voltages at the velocities U and zero respectively, and k_1 , k_2 and n are constants to be determined by fitting the calibration data.

2. Flow at the centreline of contractions

The study of the behaviour of the turbulent flow in contractions is of great interest in many engineering applications. However, most of the attention has been focused in the past on the study of the flow in axisymmetrical contractions, which for instance are used in wind tunnels design, and many numerical and experimental analyses have been accomplished on this specific type of geometry. Nevertheless, plane contractions are present in many industrial devices. For instance, the hydraulic headbox used in paper manufacturing machines is characterised by the presence of a two-dimensional contracting part, which is mounted at the end of

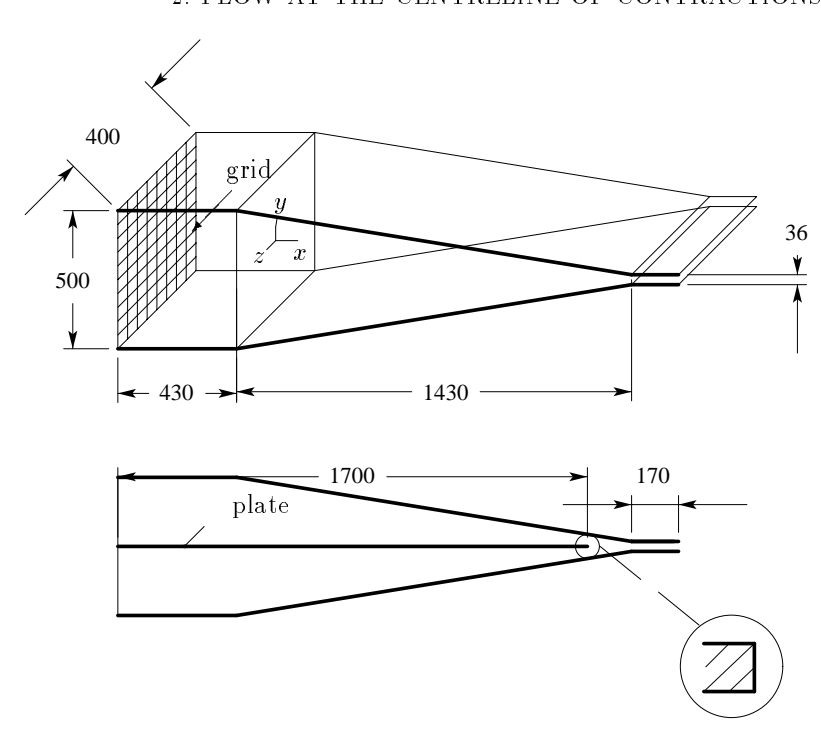


FIGURE 4.3. One sample of the experiment set-up used in the boundary layer and wake experiments, dimensions in mm.

a step diffusor. In this contraction the flow is contracted only in one direction and hereafter we call this a two-dimensional contraction. Since long time, paper manufacturers have been interested in determining the turbulence characteristics of the flow through this contraction. For instance, the mechanical properties of the paper may considerably depend on the turbulence characteristics of the flow through the headbox. In this context, the use of commercial numerical codes for the simulation of the flow inside the contraction may represent a valid tool for the design process of the device, especially if the considerably reduced costs of these numerical analyses are taken into account. However, the performance of the different turbulence models, currently available, for the flow through this geometry has not been verified.

The study of contraction's influence on turbulence characteristics begins with the work of Prandtl. He investigated the change of the intensity of the turbulent vortices in an axisymmetrical contraction according to Kelvin's circulation theorem. He simplified the transverse and streamwise components of turbulent vortices by small rectangular loops. According to Prandtl when the incompressible fluid flows quasi-one-dimensionally through an axisymmetrical contraction with x-direction as the streamwise direction in which the fluid element is extended

and y- and z-directions as the transverse direction, the side lengths $(\Delta x, \Delta y, \Delta z)$ of the rectangular vary as:

$$\Delta x \sim C, \tag{4.2}$$

and

$$\Delta y, \Delta z \sim C^{-\frac{1}{2}},\tag{4.3}$$

where C denotes the local contraction ratio defined by the ratio of the local velocity U and U_0 , the velocity at the contraction inlet, i.e.

$$C = \frac{U}{U_0}. (4.4)$$

If a fluid element moves with velocity $\vec{u} = (U + u, v, w)$, where u, v and w denote the fluctuating velocity components in x-, y- and z-direction, respectively, the conservation of circulation applied to these loops leads to the fact that the fluctuating velocity components will change according to the following expressions

$$u \sim C^{-1},\tag{4.5}$$

and

$$v, w \sim C^{\frac{1}{2}}.$$
 (4.6)

These are known as Prandtl's formulaes for axisymmetrical contractions and imply that the streamwise component of turbulence decays on passing through a contraction, whereas the transverse components grow equally.

A similar reasoning applied to the two-dimensional contraction shown in Fig. 4.1 with the coordinate system shown in this figure will lead to

$$\Delta x \sim C$$
 , $\Delta y \sim C^{-1}$, $\Delta z \sim 1$. (4.7)

Furthermore, if u, v and w are the fluctuating velocity components in x-, y- and z-direction, denoted hereafter the streamwise, vertical and horizontal components of velocity, respectively, these components become

$$u \sim C^{-1}$$
 , $v \sim C$, $w \sim 1$, (4.8)

and we denote these expressions as the results of 'classical theory'. Taylor (1935) developed the Prandtl's formulaes. He took into account the mutual interaction of continuum vortices and introduced his model of turbulence which was a three dimensional array of cubical vortices. By using the Cauchy's equations and also considering the assumption of conservation of circulation, he determined the influence of contraction, mean rate of strain, on the flow. Batchelor & Proudman (1954) and independently Ribner & Tucker (1952) used the same approach. They developed Taylor's simple model by a Fourier integral which represented the random turbulent field. Thus, they separated the random turbulent flow into a wide range of sinusoidal waves. However, in this model the fluid viscosity and the interaction between different eddies are ignored and therefore is a simplified model of real turbulent flow. These simplifications would lead to no significant error if the distortion is very rapid and therefore this model was called the 'Rapid Distortion Theory' (RDT). According to this theory, for large C the asymptotic effect on turbulence is the same as the effect of a large symmetrical contraction. This means

$$\sqrt{\overline{v^2}}, \sqrt{\overline{w^2}} \sim C^{\frac{1}{2}}, \tag{4.9}$$

which can be compared to the Prandtl formulaes for axisymmetrical contractions, expression 4.6. The explanation is that the vorticity ultimately is everywhere parallel to the line of greatest extension and the v- and w-component are produced by the same vortices, Batchelor & Proudman (1954). Noting that $U \sim C$ the development of turbulent intensities in the vertical and horizontal directions according to RDT becomes:

$$\sqrt{\frac{\overline{v^2}}{U^2}}$$
 , $\sqrt{\frac{\overline{w^2}}{U^2}} \sim C^{-0.5}$, (4.10)

2.1. Experimental study of flow through contractions. Uberoi (1954) was the first who studied experimentally the validity of the Prandtl formulaes for flow through axisymmetrical contractions. He showed that expressions 4.5 and 4.6 can hold only for C < 4 and for higher contraction ratios the streamwise turbulent component starts to increase, which is in disagreement with the Prandtl's formulaes. Hussain & Ramjee (1976) investigated four different axisymmetric contraction shapes with the same contraction ratio and showed that all the contractions affected the core flow similarly. However, the mean and turbulence characteristics of the boundary layer at contraction outlet, and the upstream influence of the contraction and the departure from isotropy within the contraction varied significantly with the contraction shape. Tsuge (1984) showed analytically that within an axisymmetric contraction only small eddies decay through the contraction in agreement with the classical theory, while large eddies are amplified with an increase in the mean velocity. This effect becomes appreciable for a contraction ratio greater than four. For two-dimensional contractions, Ramjee et al. (1972) observed a decrease of the turbulent components, however, since the maximum contraction ratio of the channel was only two, this study could not show the development of turbulence at high contraction ratios.

In order to study the effect of two-dimensional contractions on the turbulent flow, the velocity along the contraction centreline of the contraction shown in Fig. 4.1 was measured. The walls of this contraction were adjustable and therefore,

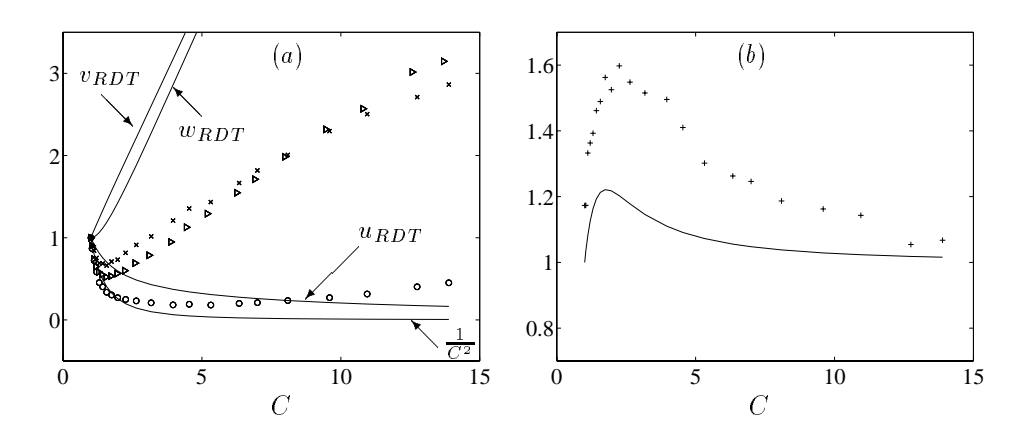


FIGURE 4.4. (a) Reynolds stress distributions along the contraction centreline of the case with grid II normalised by their inlet values. Measured data: $(\frac{\overline{u^2}}{u_0^2})$ (\diamond), $(\frac{\overline{v^2}}{v_0^2})$ (\times), $(\frac{\overline{w^2}}{w_0^2})$ (\triangleright). (—) Prandtl formula and RDT. (b) Turbulent kinetic energy distribution along the contraction centreline normalised by its inlet value: (\diamond) measured data, (—) RDT.

the effect of different contraction angles could be investigated. In order to study the effect of inlet turbulent scale two different grids with different mesh sizes were employed. To achieve isotropic turbulence the grids were mounted slightly less than 20 mesh-widths upstream of the contraction inlet. This distance was about 430 mm and 640 mm for grid gs and grid gl, respectively.

Figure 4.4a shows the downstream development of the normal components of the Reynolds stress tensor normalised by their inlet values. In these figures, the measured data are compared to the Prandtl formulaes and to the results of the Rapid Distortion Theory (RDT). The measured values of $\overline{v^2}$ and $\overline{w^2}$ are characterised by the presence of a minimum at about C = 1.6. In this region, because of the nearly isotropic condition at the contraction inlet, the production of the turbulent kinetic energy is almost zero. However, proceeding downstream the streamwise turbulent component continues to decrease reaching the minimum at about C=4. While the flow develops downstream, due to the dissipation of kinetic energy, the small scale fluctuations tend to be damped while the large scale fluctuations remain unchanged. Close to C=1.6, the rate of the decay and the production of the turbulence comes into a balance. However, further downstream, because of the unequal decay of turbulence in the vertical and streamwise directions together with the increase of the mean rate of strain, the production of the kinetic energy increases. Moreover, the production of energy in the vertical direction increases and through the pressure field the energy may be transferred to the other components. This may explain the slight increase of the streamwise

turbulent component. As far as the RDT theory is concerned it can be seen that the turbulent components distributions do not have any minimum. This is probably related to the ignorance of the dissipation of energy by this theory. Besides, the streamwise turbulent component by RDT does not rise towards the contraction outlet. This may be related to the linearisation of the equations, which can not correctly predict the distribution of the energy between the different components. It is interesting to compare the development of the *u*-component to that of the classical theory, equation 4.8, which shows that the classical theory also does not correctly predict this phenomenon.

The magnitude of the turbulent components in the vertical and horizontal directions deviated slightly due to bi-plane grids. According to Fig. 4.4b this deviation increases downstream of the contraction inlet, however these components become almost equal at high contraction ratios. This phenomenon is also predicted by the rapid distortion theory (see Fig. 4.4a), Batchelor & Proudman (1956). According to their study, when the mean rate of strain in one direction is much higher than in the other directions, the asymptotic effect on isotropic turbulence is the same as the effect of a large symmetrical contraction. In fact, when the extension in the streamwise direction is much larger than in the other directions, the vortex lines, which are responsible for the velocity fluctuation in the vertical and horizontal directions, tend to lie nearly parallel to the xaxis. The Batchelor hypothesis can imply that the vertical and the horizontal Reynolds stress components in two-dimensional contractions at high contraction ratios show the same behaviour as the Reynolds stress in the transverse direction of an axisymmetrical contraction. In Fig. 4.5a the measured vertical mean velocity, V, at three different streamwise positions, is compared to that of the potential flow. Good agreement between these data implies that the turbulence has a negligible effect on the mean flow distribution and we can conclude that U has a uniform distribution in the vertical direction, at least after a few decimeters downstream of the contraction inlet. Figure 4.5b shows the streamwise development of the measured $\overline{v^2}$ normalised by the mean streamwise velocity at the contraction inlet. These data are compared with the development of the intensity of the grid turbulence v-component using an empirical relationships, proposed by Roach (1988), for grid turbulence in a straight channel. This figure shows clearly that in the beginning of the contraction the development of the flow inside the contraction resembles that of the grid turbulence in a straight channel. This means that in this first region the turbulence behaves like a natural continuation of the development of the grid turbulence and does not feel yet the effect of the contraction. Further downstream, the measured turbulent v-component begins to rise because of the increase of the turbulence kinetic energy production in this direction and thus its magnitude deviates considerably from the curve corresponding to the homogeneous channel flow. Figure 4.6 shows the development of the vertical turbulent intensity along the contraction centreline for different grids. Because of the different turbulent intensities at the contraction inlet these



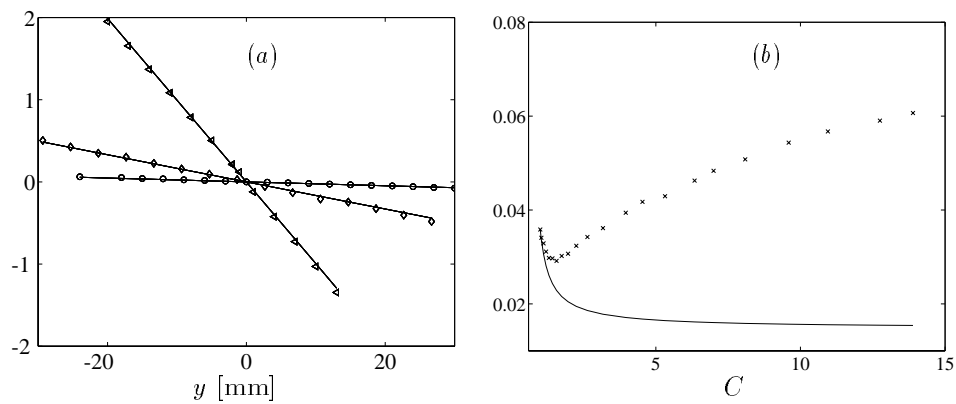


FIGURE 4.5. (a) Profiles of the mean vertical component V at different streamwise positions: measured data at x=300 mm (\diamond), x=1100 mm (\diamond), x=1400 mm (\diamond), (—) potential flow. (b) Comparison between the development of $\overline{v^2}$ along the centreline normalised by the streamwise mean velocity at the contraction inlet, (\times), with the grid turbulence development for channels with constant cross-section according to Roach (1988) (—); the same case as shown in Fig. 4.4.

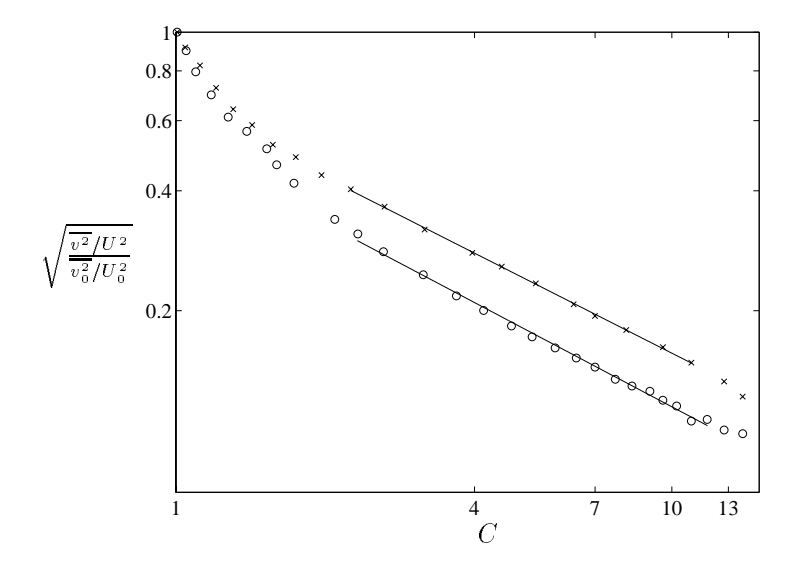


FIGURE 4.6. Development of vertical turbulent intensity along the contraction centreline scaled by its value at the contraction inlet: case with grid gs (o), case with grid gl (\times), linear fitting (—).

curves are normalised by their initial values. Immediately downstream of the contraction inlet, in a log-log graph, these curves have different slopes which can be related to different scale of turbulence at contraction inlet. However, further downstream they become almost linear and nearly parallel. The case in which the grid gs was used, had a lower inlet integral scale than the case with grid gl. In the former case, the relevant energy spectrum contains more energy in the high frequency region. This implies that the turbulence in this case contains more energy in the small scale eddies leading to an enhanced rate of energy dissipation. It should be noted that because of contracting the flow in the y-direction the scale of the eddies in this direction decreases, which can lead to higher rate of dissipation of energy. Power-law functions (C^S) were least-square fitted to the part of these curves which are linear in a log-log graph as shown in Fig. 4.6. By comparing the obtained values of S to the exponent of equation 4.10, it was observed that the turbulent intensity in the horizontal direction agrees better to the RDT than that of the vertical direction. This behaviour may be related to the dissipation rate, which is higher in the vertical direction because of the contraction of flow in this direction. The value of |S| corresponding to the v-component of the case with grid gs was larger than the case with grid gl while the horizontal components were almost equal. This can indicate that the difference in the inlet scale may have a stronger effect in the direction of the deformation. The value of |S| in the case with lowest contracting angle was largest which can be due to the enhancement of the rate of dissipation because of slow acceleration. It is obvious that this case can show the highest deviation from the RDT.

3. Relaminarisation of a turbulent boundary layer

The investigation of relaminarisation of turbulent boundary layers backs to 40 years ago when Sergienko & Gretsov (1959) observed that in compressible flow when a turbulent boundary layer became subjected to a favourable pressure gradient it reversed towards a laminar state. In an experimental work, Launder (1964) observed that the shape factor of a boundary layer subjected to acceleration increased suddenly and the local skin friction coefficient (c_f) decreased. Badrinarayanan & Ramjee (1969) studied a relaminarised boundary layer and concluded that the relaminarisation in a two-dimensional turbulent boundary layer occurs in three stages: (1) at K about 3.0×10^{-6} the turbulent bursts close to the wall disappear; (2) the breakdown of the law of the wall; and the minimum of the shape factor also seems to occur in this region; (3) about a Reynolds number, R_{θ} , equal to 300, based on the momentum loss thickness, the turbulent intensity begins to decay. However, Patel & Head (1969) showed that the shear stress distribution in the wall region rather than the Reynolds number is the most important factor for the occurrence of the boundary layer relaminarisation.

The viscous sink flow, flow in a two-dimensional contraction in which the flow is contracted only in the one direction, is of particular interest. Its laminar

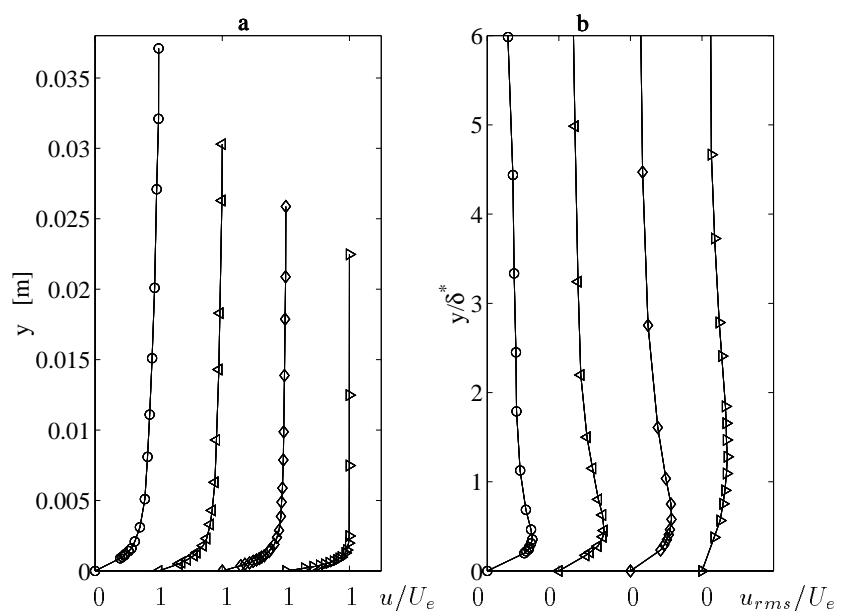


FIGURE 4.7. a) The mean velocity profile at four different downstream positions; x=0 mm (\circ — \circ); x=292 mm (\diamond — \diamond); x=760 mm (\diamond — \diamond); x=1178 mm (\diamond — \diamond). b) Non-dimensional u_{rms} at the same positions as in a.

case is one of the rare cases when the analytical solution of Navier-Stokes equation exists (Schlichting 1979). At high Reynolds numbers the flow consists of a potential core region and boundary layers along the walls. Pohlhausen (1925) solved the boundary layer equations analytically and showed that all solutions were self-similar. In the turbulent sink flow boundary layer the statistical quantities are also self-similar (Coles 1957; Bradshaw 1967). This means that the local skin friction coefficient, c_f , the acceleration coefficient, K, the shape factor, and Reynolds numbers R_{δ} and R_{θ} are independent of the position. Loyd et al. (1970) studied the development of a boundary layer in a two-dimensional contraction (a sink flow) but they did not obtain fully self-similar boundary layer. Jones & Launder (1972) studied three different turbulent flows in a two-dimensional contraction and observed that when the acceleration becomes sufficiently strong, the boundary layer relaminarises. Direct numerical simulation of the flow inside a contraction was carried out by Spalart (1986). He found that at sufficiently low Reynolds number the logarithmic layer decreases in thickness, but he could observe streaks in the wall-layer region even at the lowest values of R_{θ} for which turbulence can be sustained. Moreover, he found that the relaminarisation of the boundary layer occurs at $K = 3.0 \times 10^{-6}$

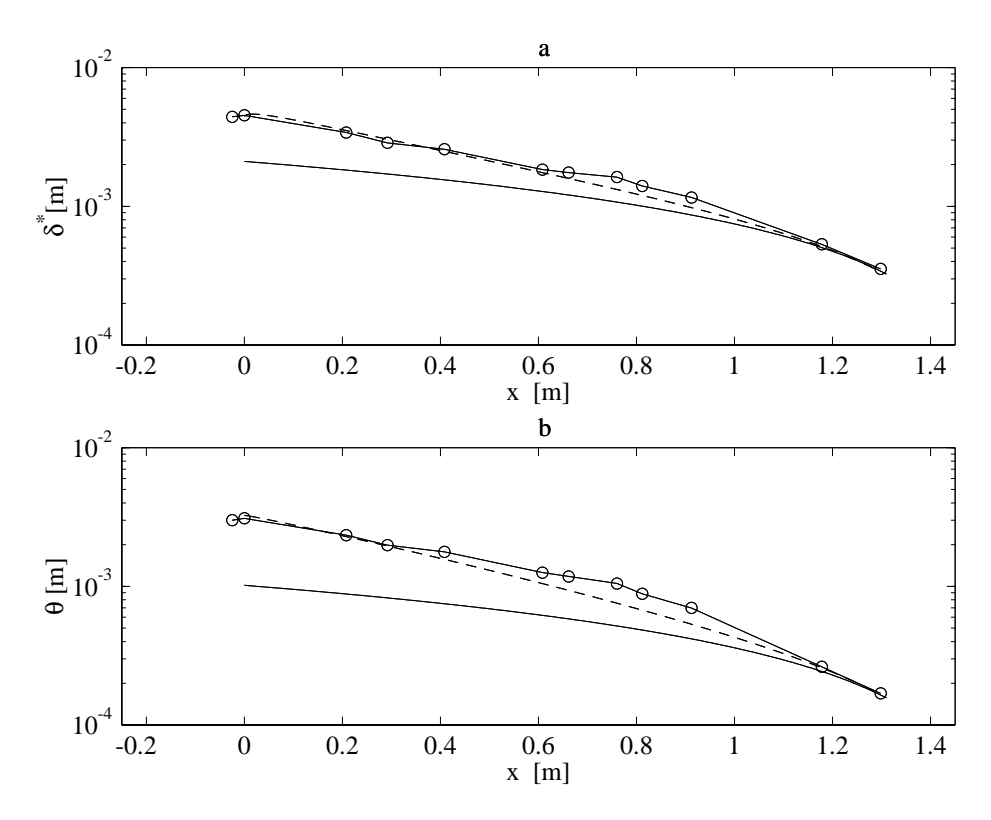


FIGURE 4.8. The downstream development of a) the displacement thickness; b) the momentum loss thickness according to: the measured profiles using grid I (o—o); the finite difference computation (- - -); the analytical self-similar laminar boundary layer (—).

3.1. The boundary layer measurement. The hot wire anemometer technique was used to measure the streamwise velocity inside the boundary layer at different downstream positions and some samples of the mean velocity and rmsprofiles are presented in Figs. 4.7a-b, respectively. The mean velocity profiles in Fig. 4.7a show that in the presence of a favourable pressure gradients the velocity defect in the outer region decreases. The first profile was measured at the contraction inlet and it was observed that this profile was fully turbulent. According to this figure, the boundary layer thickness decreases downstream and the thickness of the last measured profile became about 2 mm, which was 1/20 of that of the initial profile, which suggests that it may have become laminar. Because of this very thin boundary layer no attempts were made to measure the other fluctuating quantities such as \overline{uv} and v_{rms} . Thus, the turbulence measurements were restricted to the root mean square of the streamwise fluctuations. The u_{rms} profiles, which are non-dimensionalised with the the local displacement thickness,

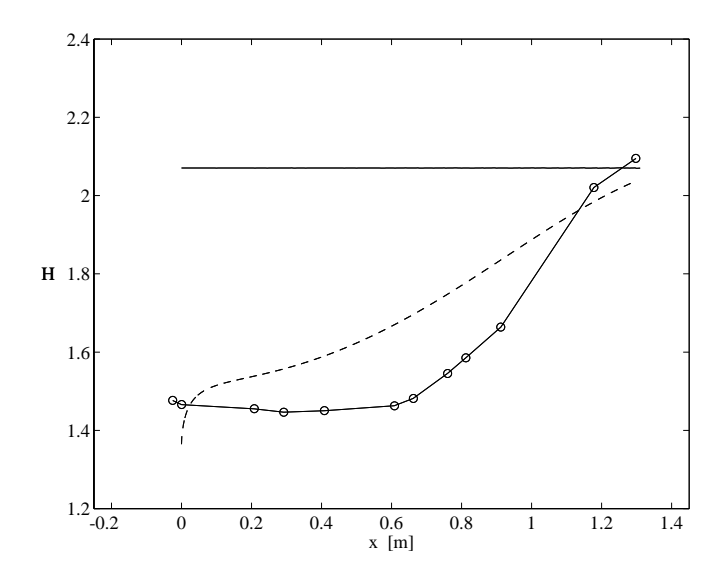


FIGURE 4.9. The downstream development of the shape factor according to: measurement (o—o); laminar finite-difference computation (- - -); analytical self-similar boundary layer (—).

are shown in Fig. 4.7b. Actually, the y-position of the point of maximum u_{rms} moves towards the wall when the flow develops downstream. However, as Fig. 4.7b shows clearly, it moves away from the wall in this non-dimensional coordinate. Thus, this can be another indication that the boundary layer goes towards a laminar state (see Westin et al. 1996).

The streamwise development of displacement thickness, δ^* , and the momentum loss thickness, θ , are shown in Figs. 4.8a-b, respectively. In these Figs. δ^* and θ from the measured mean velocity profiles are compared to both the laminar analytical self-similar solution and the laminar boundary layer computed by a finite-difference program. In the computed boundary layer the geometry was according to the set-up geometry shown in Fig. 4.3. Moreover, the measured velocity profile at the contraction inlet was chosen as the initial velocity profile for the finite-difference computation. This means that the initial profile of the computation has the same thickness as the measured profile but without its fluctuations. As is shown in Figs. 4.8a-b the displacement and momentum loss thicknesses, δ^* and θ , of the computed boundary layer are very close to δ^* and θ obtained from the measurements except in the transition region. These figures imply that all boundary layers of viscous sink flow, independent of the initial condition at inlet, develop towards the laminar self-similar state.

Finally, The downstream development of the boundary layer shape factor is shown in Fig. 4.9. In this figure the obtained shape factor from the measurements is compared to that of the laminar analytical self-similar and computed boundary layers. As it is clear from this figure the differences between the shape factors

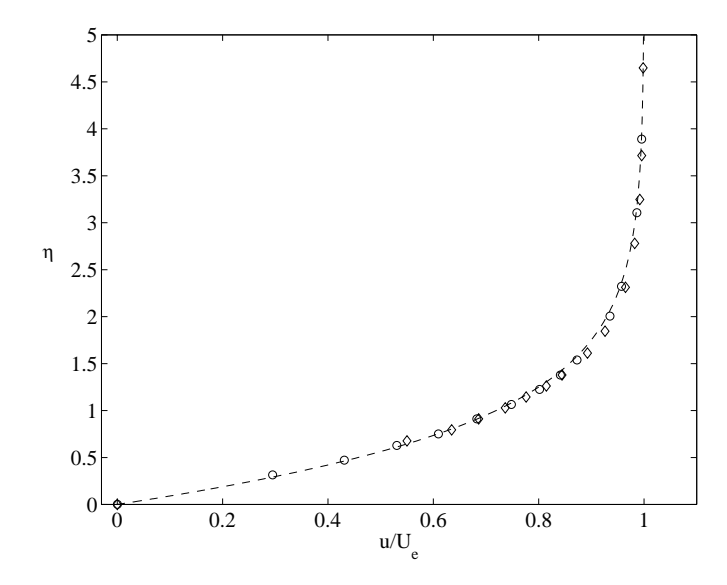


FIGURE 4.10. Velocity profiles in self-similar coordinates; (- - -) analytical laminar self-similar profile, (o) relaminarised profiles at 1178 mm, (o) at 1298 mm downstream of the contraction inlet.

obtained by different methods decreases downstream. This can also be another indication that the sink flow boundary layers with different backgrounds and initial profiles develop towards a universal condition. It is interesting to note the differences between the computed and the measured boundary layers. The sharp increase of H in the very beginning of the computed boundary layer has no physical interpretation but may be due to the fact that the wall-normal mean velocity, V, of the initial boundary layer profile has been partly guessed. However, after this short region the increase in H becomes more realistic. Before the downstream position x = 800 mm the shape factor from the measurement is almost constant whereas the shape factor obtained by computation has increased continuously. The absence of fluctuations and turbulence in the computations can be behind this increase. The turbulence in the boundary layer forces the flow to mix and therefore the momentum loss thickness decreases less than that of the computation without the turbulence. Subsequently in this region the rate of decrease in δ^* and θ are equal and the shape factor remains unchanged. Furthermore, the almost constant shape factor in this region suggests that the turbulent boundary layer in the converging channel can be self-similar because non-dimensional quantities of self-similar boundary layers are constant.

In Fig. 4.10 two relaminarised and the analytical laminar self-similar profiles are plotted in self-similar coordinates. The self-similar coordinates are defined according to

$$\eta = y \sqrt{\frac{U_e}{-\nu(x - x_0)}} ; \frac{u}{U_e},$$
(4.11)

where x_0 is the distance between the contraction inlet and a virtual point where two sides of the plane contraction meet if we let the contraction continue. In our experiment set-up, x_0 was 1543 mm. It seems that this virtual point is very important for the flow inside a converging channel and the distance to this point decides the character of the boundary layer profiles. As is obvious the measured and the analytical profiles agree well which implies the relaminarised boundary layer profiles are self-similar. Furthermore, when these profiles were plotted in the wall coordinates a good agreement was observed, too. In the sink flow studies which listed by Sreenivasan (1982), only Jones & Launder (1972) reported a self-similar laminar boundary layer. In agreement with direct numerical simulation of the flow inside a convergent channel by Spalart (1986) even in the relaminarised boundary layer the fluctuations were still present. A further study by Fornaciari et al. (2000) showed that in the relaminarised boundary layer streamwise streaks exist.

The good agreement between the mean quantities of the relaminarised boundary layer and the analytical self-similar boundary layer simplifies the estimation of the characteristics of the contraction walls boundary layer. In the next section the analytical self-similar boundary layer is used to estimate the displacement thickness of the wake, immediately downstream of the plate trailing edge.

4. Plane wakes subjected to favourable pressure gradient

As was discussed in chapter 3, a numerical study by Parsheh & Dahlkild (1997) showed that in the jet of a multi-layer headbox mixing can be limited if the plate length is chosen shorter than the contraction length. They also concluded that it is likely that a plate length exist at which the mixing is minimised. It is important to note that since the pressure gradient is variable, different plate lengths leads to different pressure gradient histories. Thus, the flat plate wakes are formed and developed subjected to a different variable favourable pressure gradient histories. This flow becomes even more complicated in combination with a channel flow following the contraction outlet. If the wake velocity defect has not fully decayed when it leaves the contraction and enter the channel with constant cross section, the turbulence level may rise significantly. It is desirable to study this kind of wake and determine, for example, its self-similarity, mean and turbulence characteristics and effect of plate length.

4.1. Measurement of wakes in a two-dimensional contraction. Fig. 4.3 shows one of the experiment cases studied in this work. The cases studied in this thesis differed to each other in at least one of the following aspects: the plate length (different pressure gradient histories), grid (different turbulence characteristics in the contraction inlet), Reynolds number, form of trailing edge

and the contraction ratio. In some of the experiment cases, in addition to the velocity measurement by CTA, the fluid layer above the plate was heated and the temperature profiles across the wake were measured by CCA technique. The temperature is considered as a passive scalar and its transport to the other layer is thus a measure of the mixing. The free-stream turbulence was generated by means of grids installed upstream of the converging channel. Each grid was mounted 430 mm upstream of the contraction inlet. In the temperature measurement a pair of heat element packages were mounted on the upstream side of grid gl at upper and lower sides of the plate. The unheated element was mounted to produce symmetric flow condition. Four different trailing edges were employed in this study where two of them were wedge-formed and the other two were square-formed.

4.2. Self-similarity of wakes subjected to pressure gradient. Townsend (1956) studied analytically and experimentally plane wakes and found that the self-similar solutions can exist for arbitrary pressure gradients if the wake velocity defect is sufficiently small. Reynolds (1962) and Keffer (1965) have shown, however, that further conditions must be satisfied. They concluded that the production of turbulent kinetic energy due to the applied rate of strain should be sufficiently small in order to obtain a self-similar wake. Narasimha & Prabhu (1971) studied plane turbulent wakes undergoing transition from an initial equilibrium state to a different condition, as a result of a nearly impulsive pressure gradient. They showed that the wake did not exhibit self-similarity when the pressure gradient was large. They concluded that a wake can be in equilibrium condition only if the streamwise strain rate is appreciably less than the wake shear. Kawall & Keffer (1982) in an experimental work studied the development of a passively heated cylinder-generated wake which became subjected to a constant rate of strain. They found that, although the scales based on mean profiles showed self-similarity, the scales based on root-mean-square profiles did not become self-similar. They concluded that the distorted wake does not undergo a truly self-preserving development and believed that this lack of self-preservation is the result of amplification, by the distortion field, of coherent structures within the flow.

Figures 4.11a-b show two samples of the mean velocity profiles in self-similar coordinates. In these Figs. U_e , U(x,y) and U_s denote the local mean external flow velocity, local mean velocity inside the wake and the wake maximum velocity defect, respectively. The wake length scale, which is denoted by l, is defined as the distance between the centreline and the position at which $U_e - U$ is $\frac{1}{2}U_s$. These profiles are compared to the function $f = \exp(-\eta^2 \ln 2)$ which is the analytical solution of turbulent self-similar wakes subjected to pressure gradient (Narasimha & Prabhu (1971)) and the function $\sec (0.881\eta)$ suggested by Mattingly & Criminale (1972). The velocity defect profiles of the case shown in Fig. 4.11b, except the profile measured one plate thickness downstream of the trailing edge, follow towards the self-similar profile, however, all the profiles presented in

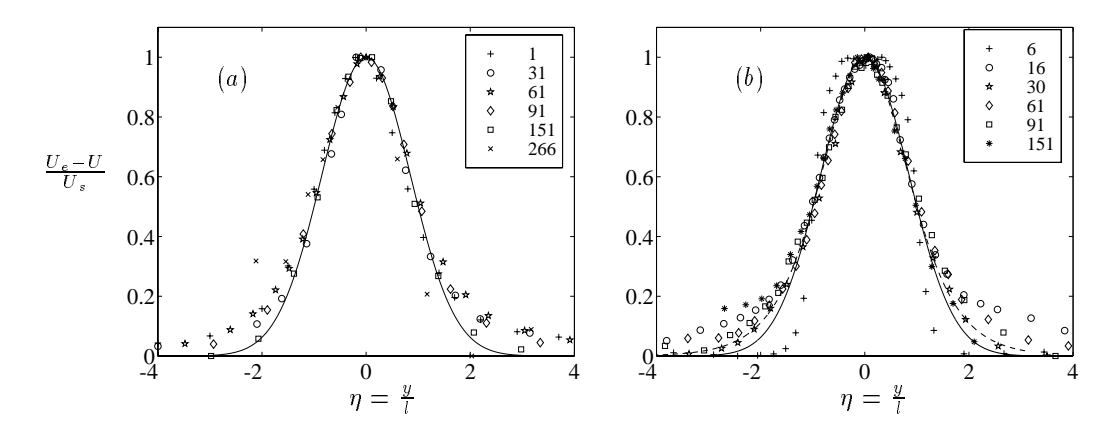


FIGURE 4.11. Velocity defect distribution in self-similar coordinates, $\frac{U_e-U}{U_s}$, versus $\eta=y/l$ compared to the analytical wake function, $\exp(-\eta^2 \ln 2)$ (—) and the function $\mathrm{sech}^2(0.881\eta)$, (- -) in a case with (a) wedge-formed (b) square-formed trailing edge. Legend shows distance to the trailing edge in mm; in these cases the distance between the trailing edge and the contraction outlet is 230 mm.

Fig. 4.11a, almost agree with the self-similar profile. In the former case the trailing edge was square-formed while in the latter case it was wedge-formed. In general, better agreement was observed with the function $\mathrm{sech}^2(0.881\eta)$. Narasimha & Prabhu (1971) defined equilibrium wakes as self-similar wakes with universal velocity and length scales. They also concluded that a shallow wake can be in equilibrium condition only if the streamwise strain rate is appreciably less than the wake shear. After using U_s and l as velocity and length scales, respectively, it was observed that none of the cases studied in this work was in equilibrium condition. However, when the Reynolds shear stress profiles were normalised with their local maximum values, $\overline{uv}/\overline{uv}_{max}$, and were plotted versus $\eta_{\tau} = y/l_{\tau}(x)$, these profiles showed almost a universal shape with exception of the profiles very close to the trailing edge. The length scale l_{τ} is defined as

$$l_{\tau} = \frac{1}{|\overline{uv}_{max}|} \int_{0}^{\infty} |\overline{uv}| dy. \tag{4.12}$$

Furthermore, the Reynolds stress component in the vertical direction of case with square-formed trailing edge, when was normalised by its maximum value and l_{τ} was used as the wake length scale, became almost self-similar, except for the profile close to the trailing edge. Thus, we can conclude that the wakes developed in a two-dimensional contraction may follow towards a self-similar

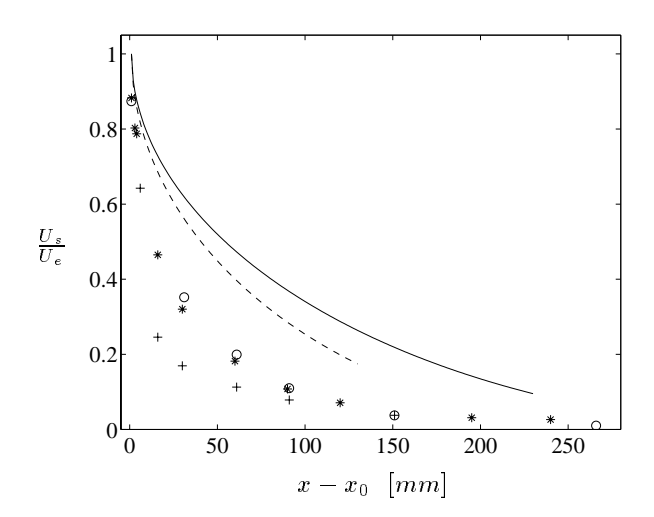


FIGURE 4.12. The downstream development of U_s in case Xd1200gl (\circ), Xd1300gl (*) and Xc1200gl (+); the inviscid U_s of Xd1200gl (-), Xd1300gl (- - -).

state but universal length and velocity scales do not exist by which all of their properties become self-similar.

4.3. Wake characteristics. Elliott & Townsend (1982) measured the characteristics of the turbulent motion in a cylinder wake when the flow passed through a three-dimensional distorting section of a wind tunnel. They concluded that substantial changes in intensity of turbulent stresses, entrainment rates, dissipation rates and turbulence length-scales occur due to the three-dimensional distortion. Liu et al. (1999) studied wake subjected to four different pressure gradients. They produced wakes with nearly the same initial conditions and subjected them to different pressure gradients: zero, constant moderate adverse, constant moderate favourable and constant severe favourable pressure gradients. They found that the pressure gradient has a large influence on the wake development in the terms of mean wake structure and turbulence quantities despite the relatively modest gradients applied. They showed that the wake width increased when the wake was subjected to the adverse pressure gradient. The larger the applied favourable pressure gradient the thinner the wake became. The intensities of different components of the turbulence of the wake subjected to the adverse pressure gradient and the severe favourable pressure gradient were largest and smallest respectively.

Figure 4.12 shows the downstream development of the ratio of maximum velocity defect, U_s , and the local external flow velocity, U_e . In this figure, U_s related to the analytical study of inviscid flow without presence of turbulence for two plate lengths are also shown. To derive the inviscid velocity defect, it was assumed that the pressure gradient inside the wake is equal to the pressure

gradient at the outer flow. As Fig. 4.12 shows, at equal distance to the plate trailing edge, the relative U_s^{inv} related to the longer plate has decayed more than the shorter case.

Owing to the recirculation of flow downstream of square-formed trailing edges, in this region the magnitude of U_s/U_e related to the wakes of these edges is larger than unity (not shown in the graph). Thus, this ratio for the case with square-formed trailing edge, in the region close to the edge, should be larger than that of the case with the same plate length and wedge-formed trailing edge. However, according to Fig. 4.12, further downstream the velocity defect of the former case has decayed more than the other case. In the case with square-formed trailing edge, the flow separation behind the trailing edge and thus a large production of turbulent energy can be behind this more rapid decay of the velocity defect. Furthermore, according to Fig. 4.12, the magnitude of U_s/U_e of the case with wedge-formed trailing edge and plate length 1300 mm is slightly larger than that of the case with the same edge and 1200 mm plate length. However, as is shown in Fig. 4.12, further downstream, U_s/U_e related to the longer plate has become smaller than the other plate. Sufficiently far downstream, where a large part of the velocity defect has vanished, this ratio is nearly equal in these cases. At equal distances to the plate trailing edge, the pressure gradient in the case with longer plate is larger than the other case, which can lead to a faster decay of velocity defect. This is in agreement with the results of Liu et al. (1999). However, when a large portion of the velocity defect is vanished the velocity defect decays in a

The effect of the type of the trailing edge on the wake development is shown in Fig. 4.13a. In the experiment cases presented in this figure, the plates had equal length and the same grid was used upstream of the contraction inlet. According to this figure U_s of the case with square-formed trailing edge decays much faster than that of a case with wedge-formed trailing edge and at the position 30 mm downstream of the trailing edge this difference is significant. However, further downstream, at 151 mm downstream of the trailing edge, the difference in U_s is negligible. As discussed earlier the high rate of decay of U_s in the case with square-formed trailing edge can be related to the turbulence level inside the wake.

The wake characteristics such as displacement thickness (δ_1) and the momentum loss thickness (δ_2) and shape factor (H) are defined as

$$\delta_1 = \int_{-\infty}^{\infty} \left(1 - \frac{U}{U_e} \right) dy, \tag{4.13}$$

$$\delta_2 = \int_{-\infty}^{\infty} \frac{U}{U_e} \left(1 - \frac{U}{U_e} \right) dy, \tag{4.14}$$

$$H = \frac{\delta_1}{\delta_2}. (4.15)$$

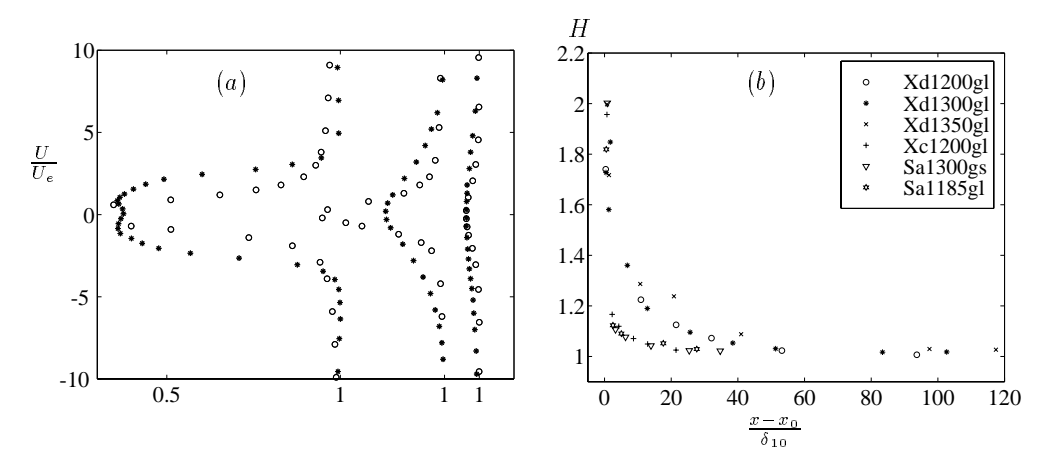


FIGURE 4.13. (a) The streamwise mean velocity profile normalised by the external flow mean velocity at of two cases with equal plate length, (*) wedge-formed trailing edge, (o) square-formed trailing edge. (b) The shape factor of the wake for the same experiment series versus the dimensionless distance to the trailing edge.

Figure 4.13b shows the downstream development of the shape factor. The quantity δ_{10} is the displacement thickness at plate trailing edge. According to this figure, the shape factor decreases downstream and ultimately reaches unity sufficiently far downstream of the trailing edge. This essentially follows from (4.13), (4.14) and (4.15) considering the limit of a small velocity defect. The downstream reduction of the shape factor can be observed to be dependent on the trailing edge type.

In Fig. 4.14 the downstream development of the maximum value of $\sqrt{v^2}$ in different cases is shown. The vertical line in this figure shows the position of the contraction outlet and x denotes the distance to the contraction inlet. As this figure shows, in the experiment cases which the distance between the plate trailing edge and the contraction outlet is short, $\max(\sqrt{v^2})$ increases sharply. This can be due to the fact that in these cases the velocity defect is not fully vanished when the flow leaves the contraction, and thus the wake has to develop without presence of favourable pressure gradient.

4.4. The analysis of mixing in the wake. Andreopoulos & Bradshaw (1980) studied the wake of a thin non-lifting airfoil. They heated one of the boundary layers and by using the temperature-conditioned sampling techniques they traced the fluid from each boundary layer within the wake. They found that the wake interaction involves significant fine-scale mixing. They also showed that

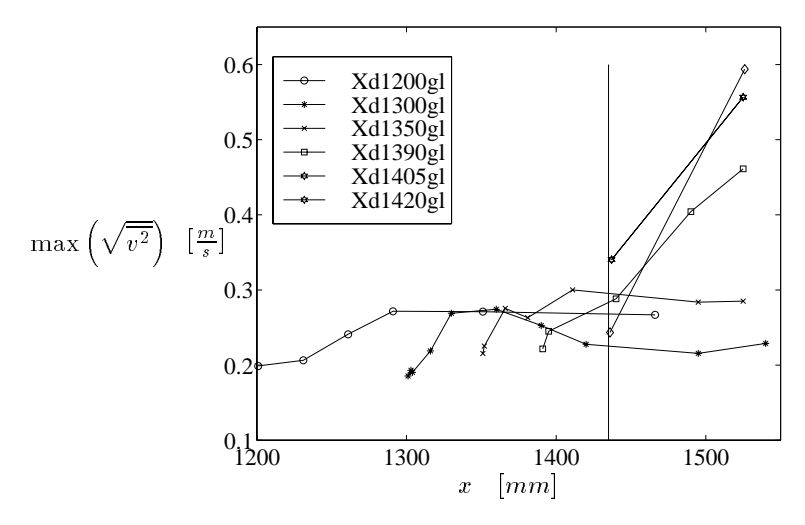


FIGURE 4.14. The development of maximum values of $max(\sqrt{\overline{v^2}})$, along the wake versus the distance to the trailing edge of different experiment cases.

the wake has a three-layer structure with a fine-scale inner wake of mixed fluid separating two layers.

Figure 4.15a shows the measured mean temperature profiles of different experiment cases 61 mm downstream of the contraction outlet, i.e inside the straight channel. The legend Xc1200gl corresponds to the case in which the trailing edge was square-formed. As the figure shows clearly, the fluid layers are almost completely mixed in this case. According to the profiles presented in Fig. 4.15a, in this position, cases in which the difference between the trailing edge and the contraction outlet was shortest, offer the lowest mixing. This was not unexpected since in these cases the warm and cold layers were in contact along a very short distance compared to the other cases. In addition, immediately downstream of the trailing edge the wake of these cases were thinnest since the boundary layer thickness decreases downstream as a result of the relaminarisation, (see Parsheh et al. (1999)). However, the passive scalar profiles at 110 mm downstream of the contraction outlet shows that the wake of long plates, particularly Xd1420gl, suffered from largest mixing, see Fig. 4.15b. This is attributed to the large magnitude of the v-component of turbulence in this case. In accordance with these results, one can conclude that the case at highest and lowest mixing depends on which position is considered, since it was shown that the case with lowest mixing at one position can offer highest mixing further downstream. In particular, it was shown that a case with short distance between the trailing edge and the contraction outlet the v-component of turbulence became large and therefore the wake suffered from significant mixing. When the distance between the plate trailing

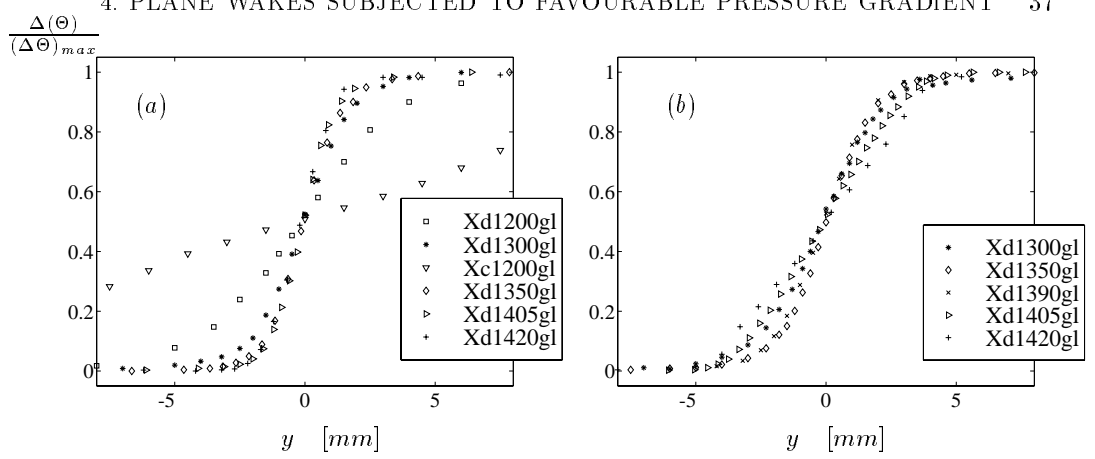


FIGURE 4.15. (a) The temperature profiles at position 60 mm downstream of the contraction outlet for different measurement cases. (b) The temperature profiles at position 110 mm downstream of the contraction outlet for different measurement cases.

edge and the contraction outlet is too long it is expected that the mixing can increase since the fluid layers are in contact a longer distance. Based on these results, depending on, at which position the lowest mixing is desirable, it is likely that an optimum plate length can be found which causes lowest mixing. The transport of passive scalar depends strongly on $v\bar{\theta}$ which in turn depends on the turbulent v-component. Thus, in order to limit the mixing of fluid layers, production of v-component should be prevented. In the cases with long plates, the velocity defect has not fully decayed when the flow leaves the contraction. As a result, the wake would develop under zero pressure gradient and consequently according to the earlier discussion the turbulence intensities will rise. The excessive production of v-component leads to a significant mixing which is not desirable.

CHAPTER 5

Concluding remarks

The computational investigation of layer mixing showed that vanes shorter than the contraction may cause lower layer mixing. Besides, an optimum plate length can exist which minimise the mixing. However, a precise computational attempt to find this vane length needs reliable turbulence models which can accurately model turbulent flow in contractions.

The measured turbulent flow at contraction centreline showed that the $K-\epsilon$ model has a very poor performance for flows with high mean rate of strain. Even, results of Reynolds stress models such as DRST and ARST showed that the turbulent component in the horizontal direction can not be correctly predicted. This can be related to the structure of turbulent flow in contractions, which can not be predicted by models based on Reynolds averaging. Besides, the results of DRST and ARST are highly dependent on the chosen rate of strain at the contraction inlet. Moreover, no model based on Reynolds averaging has successfully predicted relaminarisation of turbulent boundary layers. This is in addition to the difficulty in predicting the transition to the turbulence in laminar wakes originated from the relaminarised boundary layer. Thus, it is obvious that the models based on the Reynolds averaging are not appropriate tools for computing this kind of flow and therefore, the next step can be to use a Large Eddy Simulation (LES) model. It is important to note that the actual media in a headbox flow is the non-Newtonian fibre suspension which needs special modelling. Thus, a complete study of layer mixing must also contain a modelling of fibre suspension flow.

Finally, the measurement of turbulent flow along the contraction centreline showed that since the turbulent intensities decay downstream, the effect of background disturbances can become more significant. Thus, an accurate study requires a wind tunnel with low background disturbances. The study of the fluctuations energy spectrum was shown to be a good tool to distinguish the background disturbances from fluctuations which are the results of flow in the contraction.

Division of work between authors

Parsheh (MP) developed the computational models and performed the computations which are presented in all papers. Dahlkild (AD) contributed by useful

suggestions and many new ideas about the modelling and performing the computations and also comments on results. (MP) designed, and took part in construction of the experimental set-up and performed all the measurements. (AD) contributed to the evaluation of the measured data used in paper III and IV. Alfredsson (HF) contributed to the experiments by taking part in designing the measurement procedure used in all papers and commenting the results and suggesting new ideas in paper III. Talamelli (AT) took part in both the measurement and evaluation of data presented in paper IV.

ACKNOWLEDGMENTS

I would like to thank Docent Anders Dahlkild for his broad, accurate and generous supervision throughout the period of this work. He has taken active part in my work by proposing many ideas.

I am very grateful to Professor Henrik Alfredsson for cooperating with me to design the measurement procedure and for giving me fruitful comments on the experimental results.

This work was sponsored by FaxénLaboratoriet and I highly appreciate Professor Fritz Bark for his efforts to establish the FaxénLaboratoriet at the Department of Mechanics.

I have had the pleasure to work with Dr. Johan Westin and I would like to appreciate him for sharing his knowledge and for his useful comments. Special thanks to Dr. Alessandro Talamelli for his contribution to this study both by participation in the measurements and evaluating data of paper 4.

Part of this work was experimental and was performed at the Fluid Physics Laboratory at the department of Mechanics, KTH. I would like to send my greetings to the colleagues at the Fluid Physics Laboratory for the friendly atmosphere and thank them for helping me to learn the basic principles of performing measurement.

I wish to thank Professor Bo Norman, Dep. of Paper Technology for his important comments on application of results in Paper technology.

I would like to thank Dr. Ola Widlund, my roommates Dr. Daniel Söderberg and Mr. Tom Wright for many interesting discussions.

I am very grateful to Mr. Ulf Landén and Mr. Marcus Gällstedt for skilfully manufacturing the experimental set-up.

Especially, my best gratitude to my wife Behnoush for her love and patience and to my father and the rest of my family for their support and encouragement and to my son Shervan for being.

Bibliography

- Aidun, C., Kovacs, A. 1994 Hydrodynamics of the forming section: the origin of non-uniform fiber orientation. TAPPI 1994 Engineering conference Atlanta GA, 229.
- Alfredsson, P. H. & Matsubara, M. 1996 Streaky structures in transition. In transitional Boundary Layers in Aeronautics. (ed. R.A.W.M. Henkes and J.L. van Ingen), 374. Elsiever Science Publishers.
- Andersson, I. 1982 Simultaneous forming of multi-layer products with the KMW air wedge technology. Papex '82 International - Papermaking in the Eighties, PITA Harrowgate, Yorkshire.
- Andersson, I. 1984 Multilayering on a roll former. SPCI World Pulp and Paper Week-New Available Techniques, SPCI, Stockholm.
- Andreopoulos, J., Bradshaw, P. 1980 Measurements of interacting turbulent shear layers in the near wake of a flat plate. J. Fluid Mech., vol. 100, 639.
- Badrinarayanan, M. A. 1966 An experimental study of the decay of non-isotropic turbulence in two dimensional channel flow. J. Fluid Mech. 31, 609.
- Batchelor, G. K., Proudman, L., 1954 The effect of rapid distortion of a fluid in turbulent motion. Quar. J. Mech. Appl. Math, 7, 83.
- Baker, J. K., Beuther, P. D., & Farrington (Jnr), T.E., 1994 Impact of three dimensional headbox flows on tissue layer purity. Advances in Pulping and Papermaking, American Institute of Chemical Engineers.
- Bradshaw, P. (1969) A note on reverse transition. J. Fluid Mech. 35, 387.
- CFDS-FLOW3D Release 3.3: User Manual, CFD department, AEA Industrial Technology, Oxfordshire OX 11 0RA; United Kingdom.
- Duquesne, N., Carlson, J. R., Rumsey, C. L., Gatski, T. B. 1999 Computation of turbulent wake flows in variable pressure gradient. 30th AIAA Fluid Dynamics Conference, AIAA – 99 – 3781.
- Elliott, C. J., Townsend, A. A. 1982 The development of a turbulent wake in a distorting duct. J. Fluid Mech., vol. 113, 433.
- Ewald, J. L. 1981 Forming layered products allows best use of different furnishes. Pulp and paper (April), 137.
- Fornaciari, N., Talamelli, A., Westin, K. J. A. 2000 Experimental analysis of the relaminarization of a turbulent boundary layer subjected to a favourable pressure gradient, Tech. Rep. ADIA 2000-5, Univ. of Pisa.
- Gartshore, I. S. 1967 Two-dimensional turbulent wakes. J. Fluid Mech., vol. 30, pp. 547.
- Gence, J. N., Mathieu, J., 1976 On the application of successive plane strains to grid-generated turbulence. J. Fluid Mech., 93, 501.
- Groth, J., johansson, A. V., 1988 Turbulence reductions by screens. *J. Fluid Mech.*, **197**, 139. Herring, H. J., Norbury, N. F. 1967 Some experiments on equilibrium turbulent boundary layers in favourable pressure gradient. *J. Fluid Mech.* **27**, 541.

- Hussain, A. K. M. F., Ramjee, V., 1976 Effects of the axisymmetric contraction shape on incompressible turbulent flow. J. Fluids Eng., 98, 897.
- Hämäläinen, J. 1993 Mathematical modeling and simulation of fluid flow in the headbox of paper machines. Ph.D. thesis, University of Jyvaskyla Finland.
- Kawall, J. G., Keffer, J. F. 1982 The role of coherent structures in the development of a uniformly strained turbulent wake. Turbulent shear flow 3, Third International Symposium on Turbulent Shear Flows. Springer-Verlag, Berlin, Germany; viii+321, 132.
- Keffer, J. F. 1965 The uniform distortion of at turbulent wake. J. Fluid Mech., vol. 22, 135.
- Keffer, J. F. 1967 A note on the expansion of turbulent wakes. J. Fluid Mech., vol. 28, 183.
- Jones, W. P. 1967 Strongly accelerated turbulent boundary layers. M.Sc. Thesis, Imperial college.
- Launder, B. E. Jones W. P. 1969 Sink flow turbulent boundary layers J. Fluid Mech. 38, 817.
- Launder, B. E. and Sharma, B. T., 1974 Application of the energy dissipation model of turbulence to the calculation of the flow near a spinning disc. *Lett. Heat and Mass Transfer*, 1, no 2, 131.
- Launder B. E., Reece, G. J., Rodi, W., 1975 Progress in the development of a Reynolds-stress turbulence closure. J. Fluid Mech., 68, 537.
- Lee M. J., Piomelli, U., Reynolds, W. C., 1986 Useful formulaes in the rapid distortion theory of homogeneous turbulence. Phys. Fluids, 29, 3471.
- Linkletter, M. 1987 Tissue layering. New Technologies in Multiply and Multilayer Structures, PIRA paper and Board Division.
- Liu, X., Thomas, F. O., Nelson, R. C. 1999 An experimental investigation of wake development in arbitrary pressure gradients. 37th AIAA aerospace sciences meeting and exhibit, AIAA - 99 - 0677.
- Lloyd, M. 1997 Turbulent layer mixing during stratified forming of woodfree paper. Licentiate Thesis, Royal Institute of technology, Stockholm, Sweden.
- MacPhail, D. C., 1944 Turbulence changes in contracting and distorting passages. RAE. Aero Rept. no. 1928.
- Mellor, G. L. 1966 The effect of pressure gradients on turbulent boundary layers. *J. Fluid Mech.* **24.** 255.
- Mutama, K. R., Iacovides, H., 1993 The investigation of developing flow and heat transfer in a long converging duct. J. Heat Transf., 115, 897.
- Narasimha, R., Prabhu, A. 1972 Equilibrium and relaxation in turbulent wakes. *J. Fluid Mech.*, vol. **54**, 1.
- Norman, B. 1996 Hydrodynamic developments in twin-wire forming an overview. *Paperi ja Puu Paper and Timber* **78** (6-7), 376.
- Page, R. E., Hergert, R. E. 1989 Enhancement of paper properties and fibre economics through web stratification. Appita J. 42, (1), 33.
- Parsheh, M., Dahlkild, A. A. 1997 Numerical modelling of mixing in in stratified headbox jet.

 Tappi engineering and papermakers conference, Nashville, 1159.
- Parsheh, M. 1999 Aspects of boundary layers, turbulence and mixing in a plane contraction with elastic vanes, envisaging potential application to paper manufacturing. Licentiate Thesis, FaxénLaboratoriet, Royal Institute of technology, Stockholm, Sweden.
- Parsheh, M., Dahlkild A. A, Alfredsson H. P., 1999 Relaminarisation of a Turbulent Boundary Layer Subjected to Favourable Pressure Gradient in a Plane Contraction, Licentiate Thesis, FaxénLaboratoriet, Royal Institute of technology, Stockholm, Sweden.
- Parsheh, M., Talamelli, A., Dahlkild, A. A. 2000 Turbulence characteristics of flow through twodimensional contractions, Licentiate Thesis, FaxénLaboratoriet, Royal Institute of technology, Stockholm, Sweden.

- Patel, V. C. & Head, M. R.1968 Reversion of turbulent to laminar flow. Aero. Res. Coun. 19 859.F.M. 3929
- Pohlhausen, K. 1921 Zur nherungsweisen Integration der Differentialgleichung der laminaren Grenzchicht. Z. angew. Math. Mech. 1, 252.
- Prabhu, A., Narasimha, R. 1972 Turbulent non-equilibrium wakes. J. Fluid Mech., vol. 54, 19.
 Ramjee, V., Badr-Narayanan M. A., Narasimha R., 1972 Effect of contraction on turbulent channel flow. J. Appl. Math. Phy., 23, 105.
- Ribner, H. S., Tucker, M. 1953 Spectrum of turbulence in a contracting stream. N.A. C.A. Rep., no. 1113.
- Roach, P. E., 1987 The generation of nearly isotropic turbulence by means of grids. Heat and Fluid Flow, 8, No. 2, 82.
- Reynolds, A. J. 1962 Observation on distorted turbulent wakes. J. Fluid Mech., vol. 13, 333.
- Sergienko, A. A. & Gretsov, V. K. 1959 Transition from a turbulent to a laminar boundary layer. Translation from Russian, *RAE Trans. no.* 827.
- Schlichting, H. 1979 Boundary layer theory. McGraw-Hill, 7th edition.
- Schraub, F. A. & Kline, S. J. 1965 A study of the structure of the turbulent boundary layer with and without longitudinal pressure gradients. Stanford University, Thermo. Sci. Div. Rep. MD-12.
- Shariati, M. R., Bibeau, E., Salcudean, M., Gartshore, I. 2000 Numerical and experimental models of flow in the converging section of a headbox. 2000 TAPPI, 685.
- Sreenivasan, K. R. 1982 Laminariscent, relaminarizing and retransitional flows, Acta Mech, 44,
- Spalart, P. R. 1986 Numerical study of sink flow. J. Fluid Mech. 172, 307.
- Tanaka, H., Kawamura, H., Tateno, A. & Hatamaya, S. 1982 Effect of laminarisation and retransition on heat transfer for low Reynolds number through a converging to a constant area duct. ASME J. Heat Transfer 104, 363.
- ${\bf Taylor,\,G.\,\,I.\,\,1935\,\,Turbulence\,\,in\,\,a\,\,contracting\,\,stream.}\,\,{\it Z.\,\,angew.\,\,Math.\,\,Mech.,\,\,\bf 15,\,\,91.$
- Tennekes, H., Lumley, J. L. 1972 A first course in turbulence, The MIT Press.
- Townsend, A. A., 1954 The uniform distortion of homogeneous turbulence. Quar. J. Mech. Appl. Math Vol. VII.
- Townsend, A. A. 1976 The structure of turbulent shear flow. 2nd ed. University Press, Cambridge.
- Toyoda, K., Shirahama, Y. 1981 Turbulent near wake of a flat plate. Bulletin of the JSME, vol. 24, No. 188, 348.
- Tsuge, S., 1984 Effect of flow contraction on evolution of turbulence. Phys. Fluids, 27, 1948.
- Tucker, H. J., Reynolds A. J. 1968 The distortion of turbulence by irrotational plane strain J. Fluid Mech., 32, 657.
- Uberoi, M. S. 1956 Effect of wind-tunnel contraction on free-stream turbulence. *J. Aerosol Sci.*, 23.754.
- Westin, K. J. A., Boiko, A. V., Klingmann, B. G. B., Kozolov, V. V. & Alfredsson P. H. 1994 Experiments in a boundary layer subjected to free stream turbulence. Part 1. Boundary layer structure and receptivity. J. Fluid Mech. 281, 193.